Final Report

Calibration and Testing of Sonic Stimulation Technologies

DOE Contract No. DE-FC26-01BC15165

Reporting Period Start Date: October 1, 2001
Reporting Period End Date: December 31, 2004

Roger Turpening

Wayne Pennington

With the assistance of:
Christopher Schmidt
Sean Trisch

March 2005

Michigan Technological University

Disclaimer

Abstract

In conjunction with Baker Atlas Inc. Michigan Technological University devised a system capable of recording the earth motion and pressure due to downhole and surface seismic sources. The essential elements of the system are 1) a borehole test site that will remain constant and is available all the time and for any length of time, 2) a downhole sonde that will itself remain constant and, because of its downhole digitization feature, does not require the wireline or surface recording components to remain constant, and 3) a set of procedures that ensures that the amplitude and frequency parameters of a wide range of sources can be compared with confidence.

This system was used to record four seismic sources, three downhole sources and one surface source. A single activation of each of the downhole sources was not seen on time traces above the ambient noise, however, one sweep of the surface source, a small vertical vibrator, was easily seen in a time trace. One of the downhole sources was seen by means of a spike in its spectrum and a second downhole source was clearly seen after correlation and stacking. The surface vibrator produced a peak to peak particle motion signal of approximately 4.5 X 10^{-5} cm/sec and a peak to peak pressure of approx. 2.5 X 10^{-7} microPascals at a depth of 1,485 ft.

Theoretical advances were made with our partner, Dr. Igor Beresnev at Iowa State University. A theory has been developed to account for the behavior of oil ganglia trapped in pore throats, and their ultimate release through the additional incremental pressure associated with sonic stimulation.

Calibration and Testing of Sonic Stimulation Technologies

Final Report

Executive Summary

The track record of the sonic stimulation of oil reservoirs is, at best, irregular and uncertain. Theoretical work, some of it performed on this contract, gives us a glimpse of why that performance is so variable, namely it will work well only under a very narrow range of conditions, which rarely occur, although it will work weakly under a range of conditions, given a strong enough source.

One of the many parameters needed in any performance analysis is the strength and frequency band of the seismic source being used to do the stimulation. Under this contract, we have begun a catalog of such sources by organizing the elements needed for rigorous testing and conducting four tests under identical conditions.

In conjunction with Baker Atlas Inc. Michigan Technological University devised a system capable of recording the earth motion and pressure due to downhole and surface seismic sources. The essential elements of the system are 1) a borehole test site that will remain constant and is available all the time and for any length of time, 2) a downhole sonde that will itself remain constant and, because of its downhole digitization feature, does not require the wireline or surface recording components to remain constant, and 3) a set of procedures that ensures that the amplitude and frequency parameters of a wide range of sources can be compared with confidence.

Because sonic stimulation is the underlying interest in this study, we focused on the signal strength of a single activation of sources, recording its signal for analysis of signal strength as a function of frequency. Furthermore, to make source to source comparisons valid we sought to keep every parameter of the tests constant, except for the source. We also determined during the course of the contract that the ambient noise levels seen at the test site used are very good, and compare favorably with Michigan's seismic noise floor.

Four seismic sources were deployed at the Michigan Technological University's Reservoir Characterization Test Site in the 2003-2004 time period. Three of them were downhole sources and one was a surface source. The downhole sources included one piezo-electric vibrator and two oscillating water-jet types of tools. The surface source was a small hydraulic vibrator. They were all recorded by a downhole receiver containing calibrated geophones (three-component) and hydrophones. The seismic traces were analyzed in the time domain and in the frequency domain. The three downhole sources could not be seen above the ambient noise levels of the site in the time domain, but the surface source was easily observed. (The piezo-electric downhole source transmitted a coded signal – a "sweep" of frequencies, which could be observed in the time domain after cross-correlation, providing confidence in the analysis techniques.) The surface source, the downhole piezo-electric vibrator, and one of the downhole water-jet sources could be observed in the frequency domain.

The frequency band of the sources varied from a low of 18Hz (the low end of the surface vibrator's sweep) to a high of 1,600 Hz (the high end of the downhole piezo-electric

source's sweep). The peak to peak noise levels at our site varied from 10^{-6} cm/sec to 10^{-5} cm/sec.

Much attention has been given to the possibility of vibratory mobilization of residual oil, although there has been lack of understanding of an underlying physical mechanism that could explain variable field experiences. Such a mechanism has been found in the physics of capillary entrapment of oil ganglia, as a result of the partnership between Michigan Technological University and Iowa State University under this project. The residual oil is entrapped because of the resisting capillary forces that prevent free motion of a non-wetting fluid. A finite external pressure gradient, exceeding the "capillary-barrier" threshold, needs to be applied to carry the ganglia through. The application of vibrations is equivalent to the addition of an oscillatory "inertial" forcing to the constant pressure gradient. When this extra forcing acts along the gradient and the threshold is exceeded, instant "unplugging" occurs and at least one end of the ganglion may move through the constriction, while, when the vibration reverses direction, the flow is still plugged and the ganglion only partially moves back. This asymmetry creates an average non-zero flow over one period of vibration, explaining the mobilization effect. Minimum-amplitude and maximum-frequency thresholds apply for the mobilization to occur. The criteria of a ganglion's mobilization involve the parameters of both the medium (pore geometry, interfacial and wetting properties, and fluid viscosity) and the oscillatory field (amplitude and frequency). The medium parameters vary widely under natural conditions. It follows that an elastic wave with a given amplitude and frequency will always mobilize a certain subpopulation of ganglia leaving others intact; in this sense, the vibratory field will *always* produce a certain mobilization effect. The exact macroscopic effect will nonetheless be hard to predict, as it will represent a cumulative response of the populations of ganglia with unknown parameter distributions. Variability of reservoir responses to vibratory stimulation should thus be expected.

Experimental

Background

If the theoretical investigations of sonic (seismic) stimulation of oil production are to be applied then knowledge of the far field radiation of seismic sources is needed. This report describes the measurement of the seismic radiation of a few sources that participate in the sonic stimulation market. The field studies of the sources were conducted in association with theoretical work, and a new contribution to the theoretical literature surrounding sonic stimulation is also presented here. No measurements of oil production were made in conjunction with our seismic data acquisition and theoretical research program.

It was the purpose of this study was to establish the place, procedures, and hardware necessary for a rigorous far-field measurement program and to keep all such parameters constant. The output of this effort would be a catalog of the amplitude and frequency characteristics of sources. Funding was not available to measure every seismic source used in sonic stimulation; in fact the total number of such sources varies over time. In addition, theoretical understanding of the desired frequency content in a sonic stimulation source also varies over time, and our theory (by Beresnev, Pennington, and Turpening), presented in Appendix A, favors low frequency sources. Nevertheless Michigan Tech and their subcontractor, Baker Atlas, created a hydrophone/geophone recording system with the broadest bandwidth possible anticipating sources as yet unseen.

A quiet recording site in fast carbonate formations (low attenuation) was chosen such that weak sources could be recorded. However, the distance between source and receivers was chosen to be large (1,875 ft) such that large amplitude downhole sources could be accommodated. Glacial till covers the site making it also possible to record strong surface sources at comparable raypath distances.

Despite preplanning it was anticipated that new sources could step forward at any time forcing changes to the data acquisition parameters. However, as mentioned above we seek to keep all recording parameters constant, therefore the field program was divided into two segments, with a workshop held between the field segments. Here, we expected new sources or considerations requiring modifications to our recording parameters would be brought forward. We planned to change the recording system and parameters to encompass, as much as possible, all sources. This modified recording system would then be the constant, fixed system to be used for all measurements in the upcoming years.

This scenario played out as planned, albeit at a slower pace than expected. New sources did present themselves at our mid-program workshop but only one followed through by participating in the second data acquisition session. However, as this contract is closing, major new sources are showing strong interest in joining our measurement program. Obviously, industry funding will be necessary for this third data acquisition program but this does indicate that DOE's initial concept was correct, namely the catalog of borehole sources would be self perpetuating after being jump-started with government funding.

Need to Measure Sources

Theoretical and laboratory investigations of the sonic stimulation phenomena have continued at a slow, steady pace. This research program has made a contribution to that literature (Appendix A). Such studies usually generate an estimate of the amplitude and spectral band of the seismic motion that must be applied to the rock matrix and pore fluid before the proposed phenomenon takes place. This in turn raises the questions about the actual signal amplitudes and spectral bandwidth generated by today's array of stimulation sources. Are they strong enough to be effective, or conversely, what is the effective radius for a given source?

Whereas the frequency band for any seismic source is commonly discussed and cited in scientific and marketing literature, its signal strength is rarely documented. Statements about signal to noise ratios, useful depths of penetration, and usage in benchmark areas of the world are commonplace, however, no reference is given to an amplitude in absolute units at fixed distance from a source. The Navy, of course makes exhaustive measurements on acoustic sources and the same can be said for airguns used in marine seismic work. However, here we are interested in those sources that claim to be useful in the field of sonic stimulation.

Creation of a Test Facility

Several sonic stimulation seismic sources are used in the borehole; therefore, a borehole data acquisition system is necessary to measure their performance. The same system can be used to measure the signal power and amplitude of surface sources. At the mid-program review (June 2004, Tulsa, OK) for this contract it was suggested that surface sources will be more useful in sonic stimulation than borehole sources and should be included in our study.

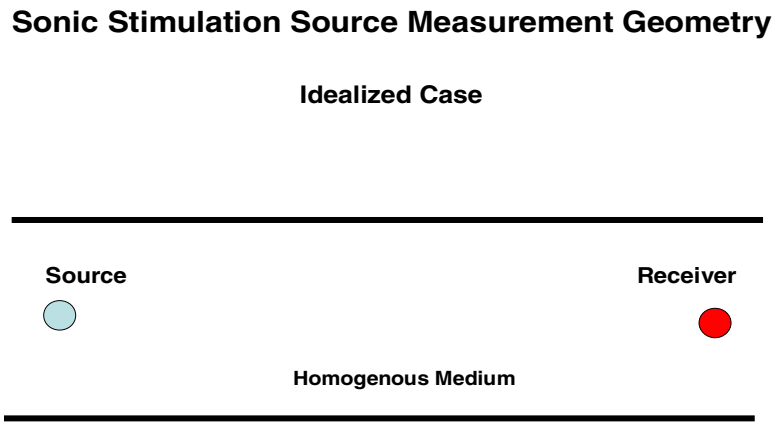

Figure 1 Desired but unrealistic situation for testing of downhole sources.

There are two major components to a test facility, first, boreholes that will remain constant and, secondly, a data acquisition system that will remain constant. A suitable test site must have at least two boreholes that are always available and for any length of time, and they must remain constant for an indefinite period of time, i.e. no engineering changes. Michigan Technological University (MTU) possesses such a site.

The data acquisition system must also remain constant. BakerAtlas, as a partner, in this research program, has developed a dedicated downhole sonde that they can deploy. This sonde digitizes the data downhole therefore the wireline and surface system need not remain constant.

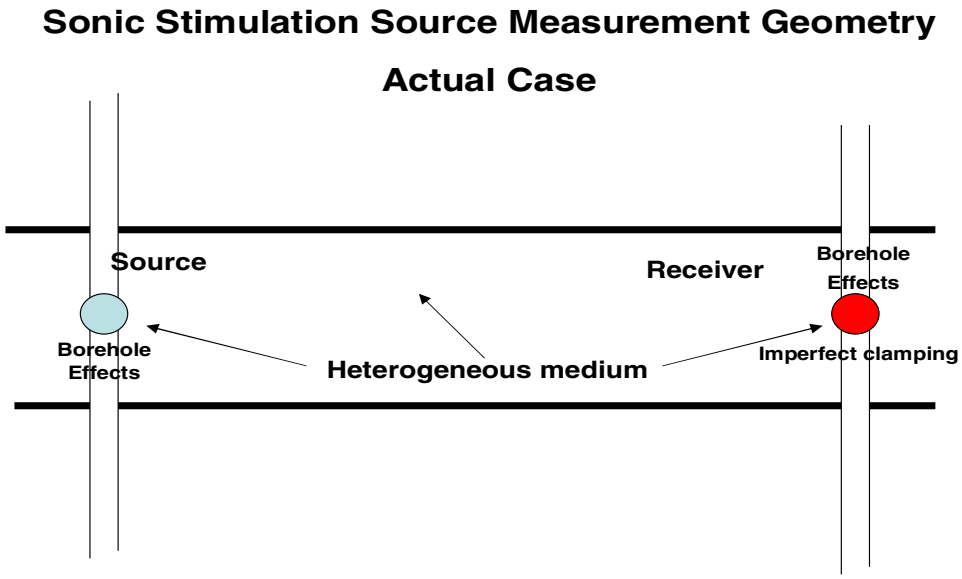

Figure 2 Schematic description of the geological, geophysical, and engineering factors that effect seismic amplitudes. For the calibration and testing of downhole seismic sources we keep all of the above imperfections constant and change only the source.

Test Geometry

Conceptually, the ideal test geometry is simple. Place the source a large horizontal distance away from a receiver both in the middle of a thick, homogenous, high velocity layer (Figure 1). Specifically, the layer is the Traverse Limestone and the middle of that layer occurs at 1,485 ft and at that depth the source and receiver will be in boreholes that are 1,800 ft apart. It is well known that the layer is not homogeneous and the boreholes influence both the radiation pattern and strength of the source and the reception patterns of the receivers. In addition there is an unknown transfer function between the borehole wall and the clamping geophone (Figure 2).

Fortunately, our task was to compare sources, thus we compensated for these deviations from the ideal by keeping every parameter, except the source itself, constant. We returned to this test site for every measurement. We placed every source in the same

borehole at the same (1,485 ft) depth. We used the same receiver at the same depth (1,485 ft) in the same borehole as every other receiver.

Beyond these efforts we instituted additional redundancies designed to find and avoid anomalous measurements. For example, in each borehole we moved the source and receiver down to 1,515 ft and repeated the measurement This is a duplicate set of measurements in case we should find an anomaly in the primary set. We also reversed the geometry for some tests, exchanging the wells used for the source and receiver.

The Michigan Borehole Research Facility—the Standard Site for Source Comparison

Michigan Tech's Test Site in the northern reef trend of Michigan was selected as the site of the source measurements for several reasons. In principle any location could be used for this type of program, it is only important that the site remain constant. In a practical sense, especially for borehole measurements, this is a very severe restriction and one of the central reasons that the Michigan Tech Test Site was chosen. Boreholes are very expensive facilities and those that are producing hydrocarbons are not available for research or, in this case, the creation of a system of standards.

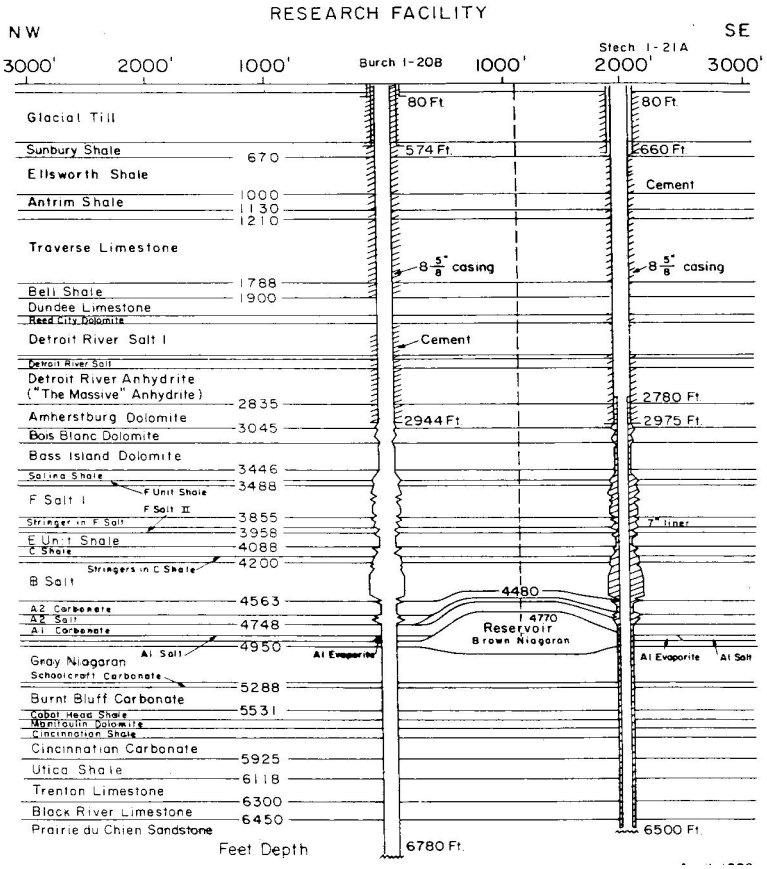

Figure 3 Cross section of the MTU Test Site. Multiple strings of casing are not present. The lower portion of the MTU/Burch borehole is left open for research purposes .

At the MTU test site (Figure 3) the boreholes were drilled for geophysical imaging research, not for oil production; one (Burch) in 1985-1986 and the other (Stech) in1990-1991. In like manner the casing design was chosen with borehole geophysics in mind, not economy. Therefore, double strings of casing were avoided with both casing and the liner fully cemented. The deeper section of the Burch borehole has been left open to facilitate open hole research. The three dimensional position of the boreholes has been determined by use of multiple runs of borehole gyroscopes (Figures 4 and 5), thus the distance between the boreholes is precisely known.

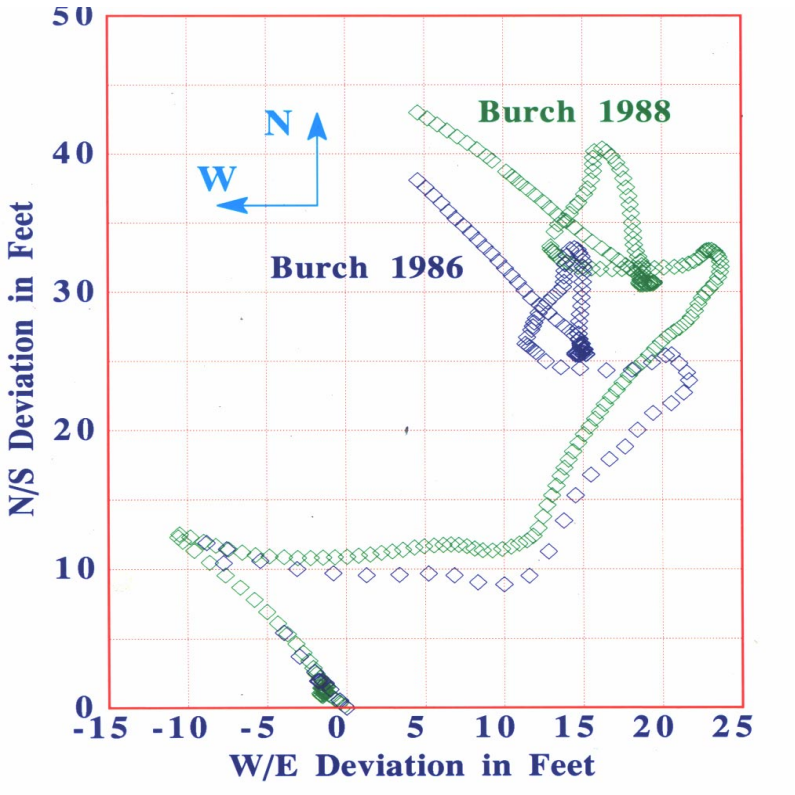

Figure 4 Two gyroscope surveys in the MTU/Burch borehole. The 1988 survey is the accepted position of the borehole because it was run with a finer level spacing.

The site is seismically quiet. The research facility is in a rural area surrounded by a state forest; therefore little seismic noise is generated on the surface. Because the boreholes never struck hydrocarbons there is no source of noise at depth outside boreholes, such as gas migrating behind the casing. In rare instances (three or four times in twenty two years) drilling in the general area produces noise for a short period of time.

One of the primary reasons that the research facility was located in Michigan's Lower Peninsula was the simple, flat nature of the earth structure. The other reason is the fact

that the reef can be used as a target for imaging research purposes. But, here in the creation of a new standard, it is the flat lying structure that appealed to the investigators. The flat lying structure of Michigan is predominately carbonates. The low attenuation of those limestones, dolomites, and anhydrites coupled with the low noise background makes this site ideal for the source comparison task undertaken here. Equally important is the fact that the site is available any time and for any length of time

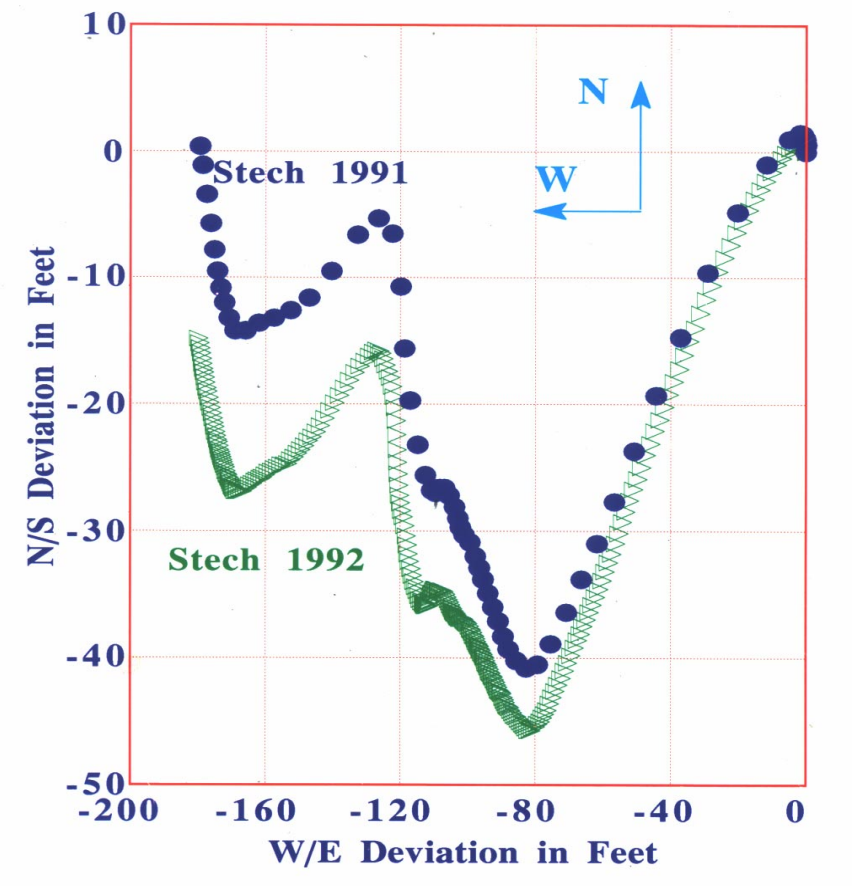

Figure 5 Two gyroscope surveys in the MTU/Stech borehole. The 1992 survey is the accepted position of the borehole because it was run with a finer level spacing and it was run with GyroData Inc.'s 'centrollers' forcing the gyroscope to occupy the centerline of the borehole.

The structure of the earth is, in the main, defined by the velocity parameter. Every seismic technique (3-D reflection, vertical seismic profiling (VSP), cross well surveys) produces a velocity map enroute to its imaging goal and all are available here in addition to conventional logs. A velocity structure (Figure 6) derived from those data was used in the numerical modeling for this project.

The Test Region--The Layer Chosen

The Traverse Limestone was chosen as the layer in which both downhole sonic stimulation sources and the standard sensor sonde would be deployed. Several

considerations went into this selection. First, recall that our first series of tests involved a hole to hole swap of source and receiver positions and secondly, most downhole sources must, or should, be deployed in a cased hole. Thus in order to satisfy both conditions the test region must be above 3,000ft

Then in that depth range we sought a thick homogenous layer that would present identical conditions surrounding each borehole. Furthermore, we knew that there are some small zones of poor cement in the Burch borehole and we wished to avoid those depths. We

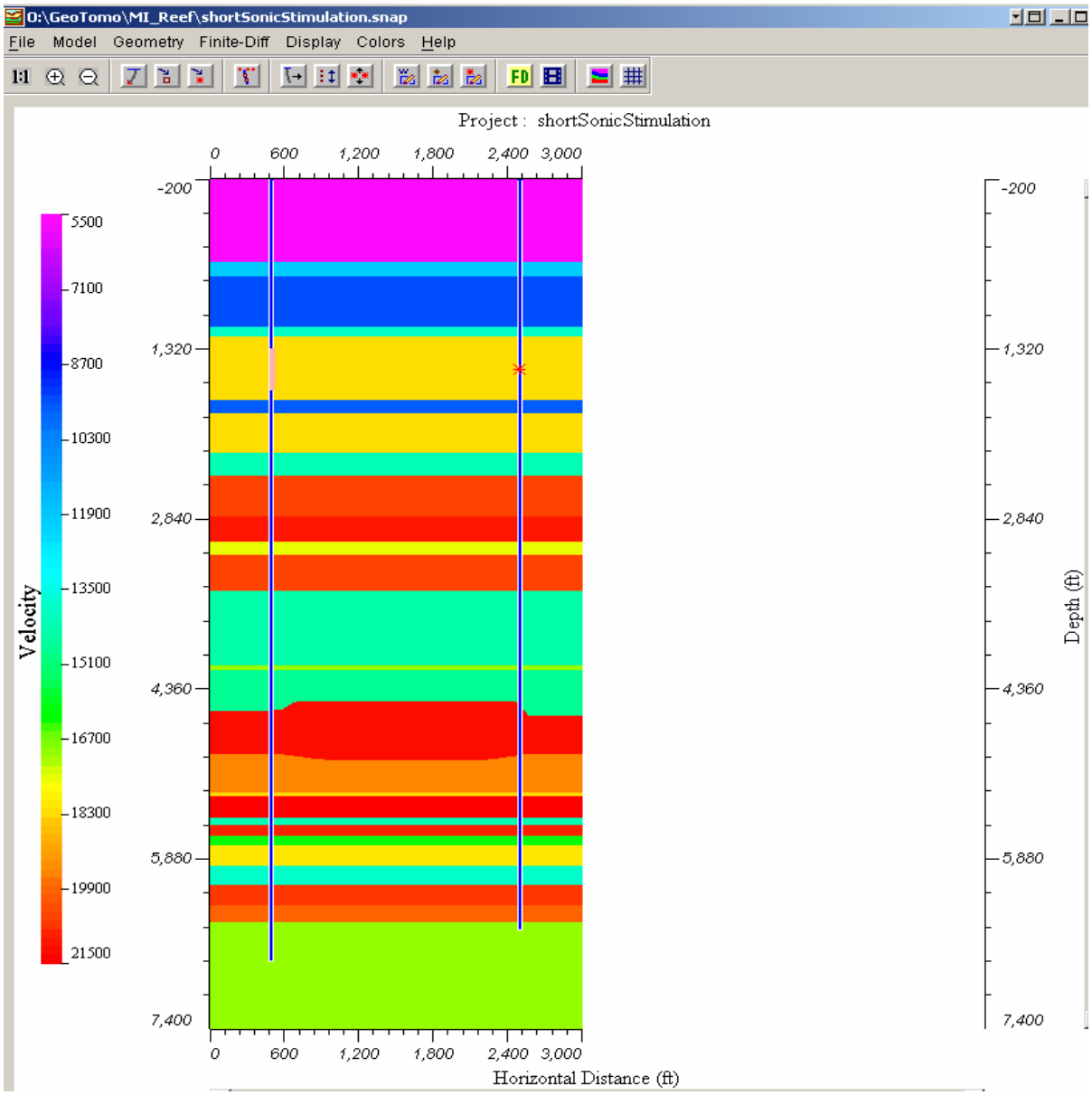

Figure 6 The velocity structure used in the numerical modeling of seismic wave propagation expected from downhole sources at the Michigan Technological University's Reservoir Characterization Test Site. The above gyroscope surveys place the boreholes 1,875 ft apart at a depth of 1,485 ft

selected two depths within the Traverse Limestone again for redundancy purposes and our well logs in both holes guided us to 1,485 ft and 1,515 ft At these depths there is a minimum of variation between the limestone surrounding each hole.

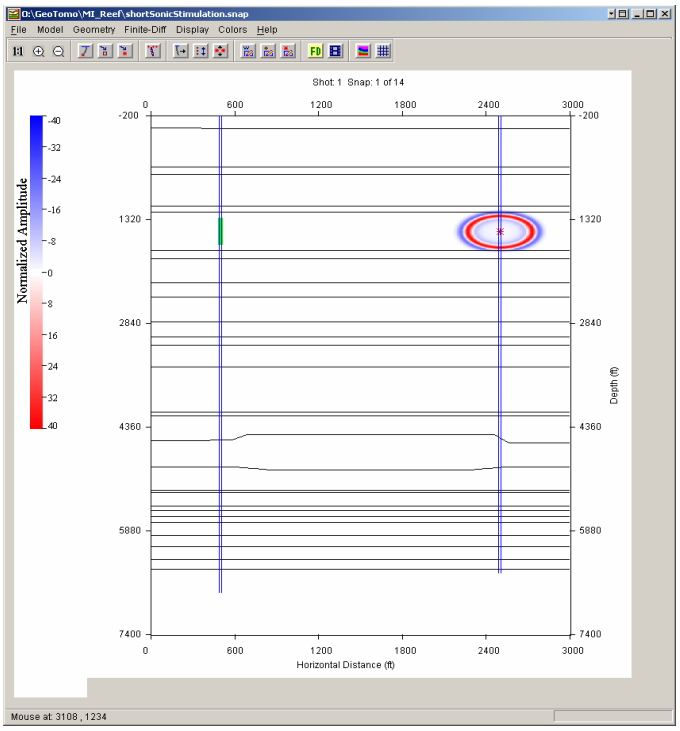

Figure 7 Time = 0.020 seconds

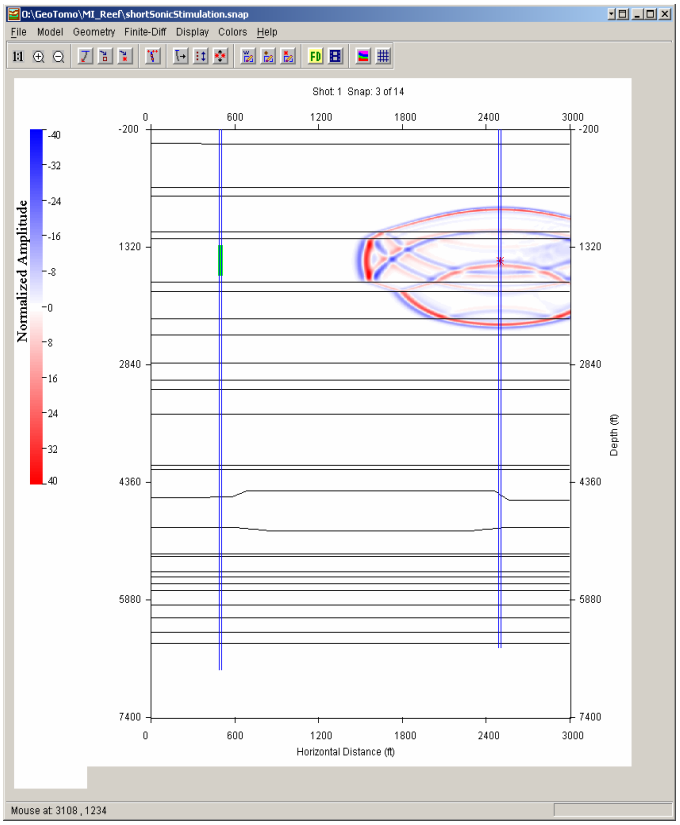

Figure 8 Time = 0.040 seconds

Numerical Modeling of Seismic Wave Propagation for this Geometry

The seismic wave propagation expected for our geometry is displayed here in Figures 7-11 There in time steps of 0.020 seconds one can see that the first arriving energy has propagated horizontally through the Traverse Limestone with reflections making up the later arrivals. The velocity structure used was obtained from the master model of the test site built from two decades of seismic measurements at the site. The recording of the Baker Atlas piezo-electric source in this research program has given us a new velocity in the horizontal direction through the Traverse Limestone (17,860 ft/sec). This differs from the acoustic logging data which has propagated vertically through the layer.

With this modeling capability we can correctly identify the arrivals of all impulsive sources if the firing instant (zero time) of the source is known. This is valuable if we wish to use the energy in the first arrival as the unit of source comparison.

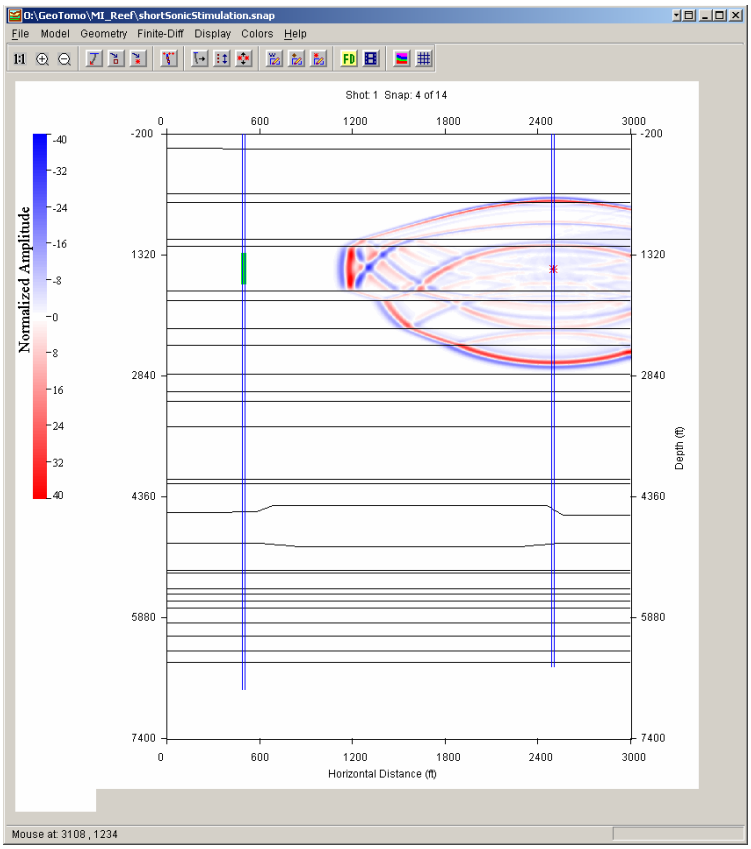

Figure 9 Time = 0.060 seconds

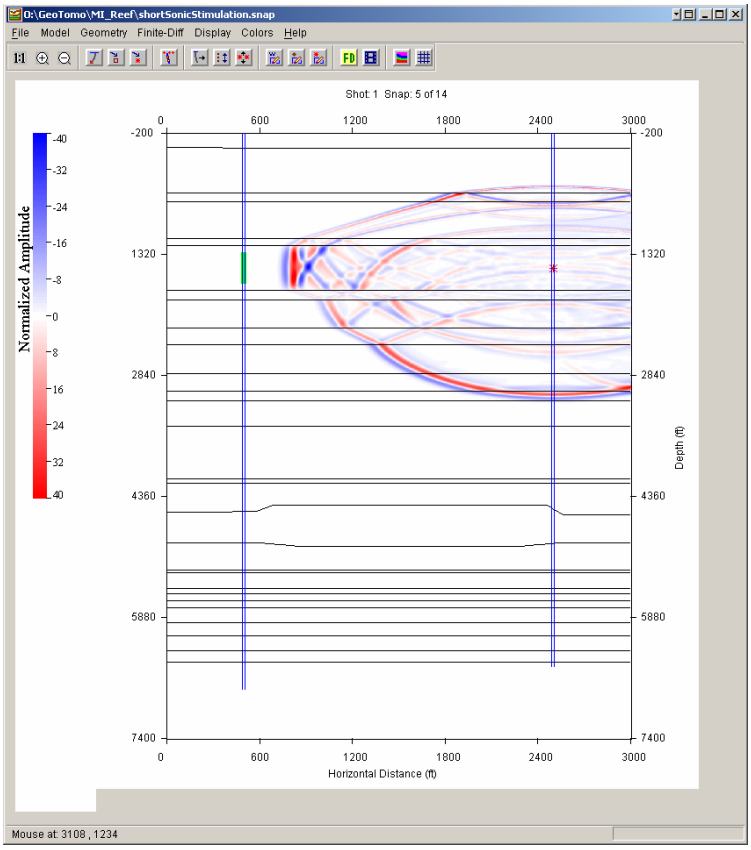

Figure 10 Time = 0.080 seconds

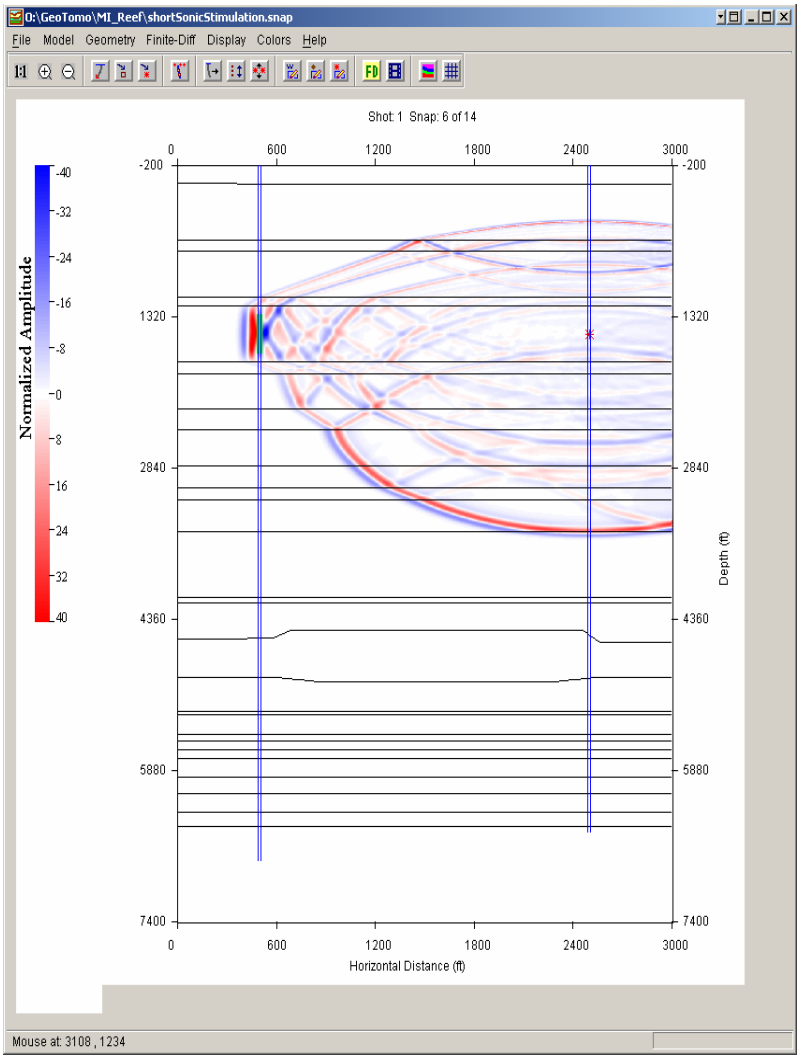

Figure 11 Time = 0.100 seconds

The Recording System

To accomplish the recording task Michigan Tech entered into a partnership with Baker Atlas Inc. Baker Atlas has broad experience in well logging and borehole seismology. In this research program we sought their expertise in downhole recording with clamped geophones and hydrophones. We wished to develop a sonde that could cover the entire range of frequencies presented by the known sources and any new sources that might be developed over the life of this standard. Furthermore, we wanted that sonde to remain constant and available over the life of our standard. Additionally, we requested redundancy, i.e. multiple three component geophones and multiple hydrophones such that we could spot any anomalous data and so that any one sensor failure would not force us to abandon a field recording session.

Hydrophones

Hydrophones are useful in the high frequency range (hundreds of hertz to several kilohertz) while geophones span the low frequency range (a few hertz to one to two hundred hertz). The sonde uses two hydrophones, one of which is recorded with two gains separated by 20db, resulting in three hydrophone channels used. The sensitivity of each hydrophone is approximately 1.7×10^{7} Volts/microPascal. The output of one hydrophone is then amplified with 60db of gain while the other hydrophone is amplified by 60 db of gain for one channel and 40 db for another channel. An anti-aliasing filter with a gain of unity was then applied before sampling the data at 4,000 samples per second (1/4 millisecond sampling rate) The resulting signals were then digitized downhole with a 16 bit A/D converter and transmitted up the wireline.

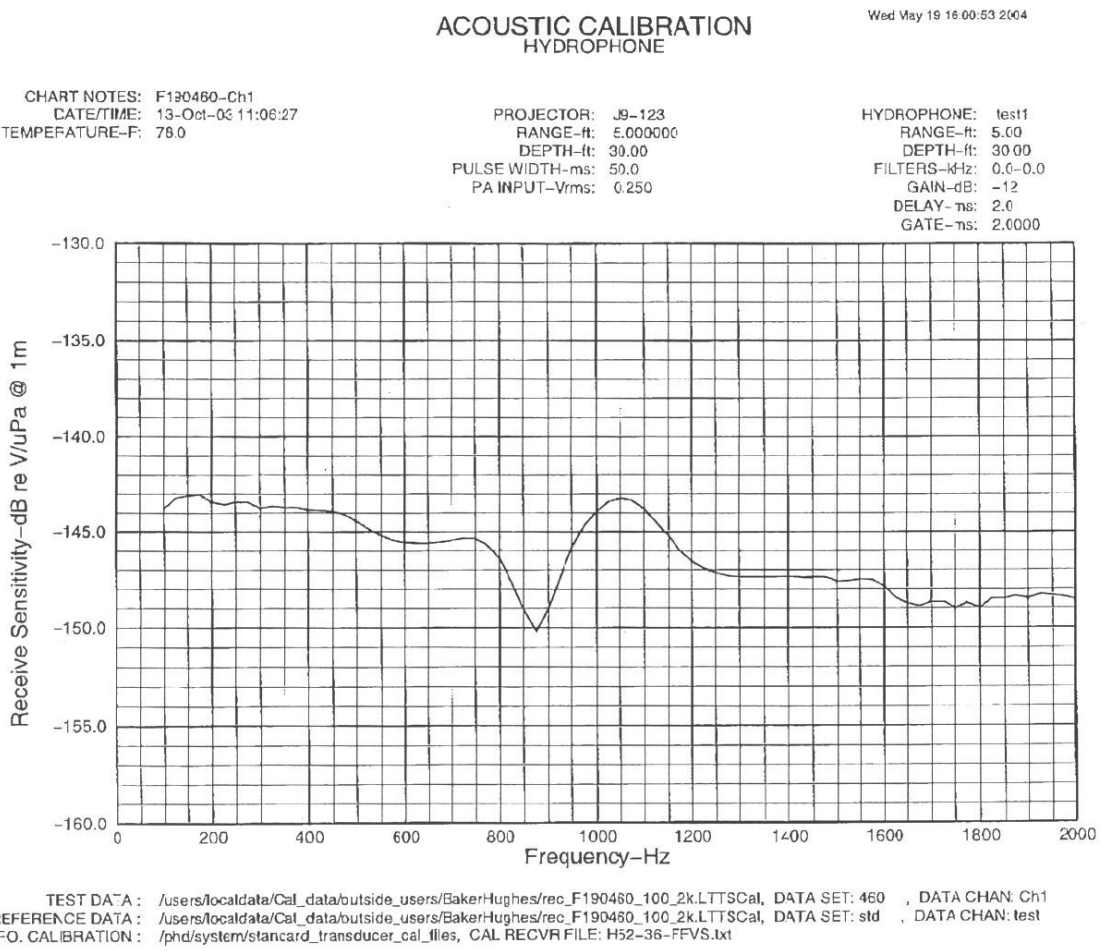

Figure 12 Typical sensitivity curve for the hydrophones in the Baker Atlas sonde.

Geophones

Six #1011 geophones (two three-component packages) were used. Each geophone had a sensitivity of 975 mVolts/in/sec of particle motion. Each geophone was amplified by 60 db of gain (a factor of 1,000). An anti-aliasing filter with a gain of unity was applied. The resulting signals were then sampled at the rate of 4,000 samples per second (1/4 millisecond sampling rate), digitized downhole and transmitted up the wireline. Because the signals are digitized downhole the resistance of the wireline does not affect the amplitude of the signals, i.e. we need not be concerned about maintaining the same wireline for all data acquisition programs.

Recording System

Wireline and mast trucks were supplied by the Mt. Pleasant, Michigan office of Baker Atlas Inc. All of the data were recorded on Baker Atlas's Seismic Logging System 3 recording system (SLS III) and then passed on to Michigan Tech on CDs, along with the observer's notes.

Data

Clean Wells Ltd. Tool

The Clean Wells Tool is a perforation cleaning device, deployed on tubing, that emits an oscillating stream of water under high pressure. The frequency of the oscillation is controlled by the mechanical design of the tool. Fluid pressure and flow rate can be varied at the surface and, indeed, they were varied in our tests over the following three sets of parameters:

Pressure	Flow
1,000 psi	26 gallons per minute
1,575 psi	36 gallons per minute
1,600 psi	36 gallons per minute
2,000 psi	42 gallons per minute
2,100 psi	42 gallons per minute

As described above, we deployed this source at two depths: first in the MTU/Stech borehole (1,485 ft and 1,515 ft) and then again at the same two depths in the MTU/Burch borehole. The receiver sonde was clamped at the same two depths in the opposite borehole each time. This source is continuously radiates energy. It is controlled by the pump on the surface, which could not be turned on or off instantaneously; therefore, we recorded segments of data seven seconds long when the source was on. In addition we recorded seven-second segments of data when the source was off, providing measurements of ambient noise.

Data

Given the nature of this source, we were looking for a continuous signal with a constant frequency in our seven-second units of data. Neither the geophone traces nor the hydrophone traces, when viewed broad band or filtered, showed any obvious signal. However, after examining the spectra of the records, when the source was on, a spike was noticed around 260 Hz when the source was operating at 1,000 and 1,535 psi. The spike was visible on both hydrophone and geophone data, but especially strong on the hydrophone data. The same filters were run on the ambient noise and we found no such spike. Taking these together strongly suggested that the Clean Wells Source produced a narrow band signal around 258 Hz.

With a signal detected only in the spectra of hydrophone and geophone data, its amplitude (1,875 ft from the source) must be at or below ambient seismic noise levels. These levels can be stated to be approximately 10^{-5} cm/sec in particle motion and 10^{-7} μPa in pressure.

The data and spectra from selected receivers as deployed at 1,485 ft in the MTU/Burch borehole are shown here, for the test associated with the Clean Wells Ltd. tool.

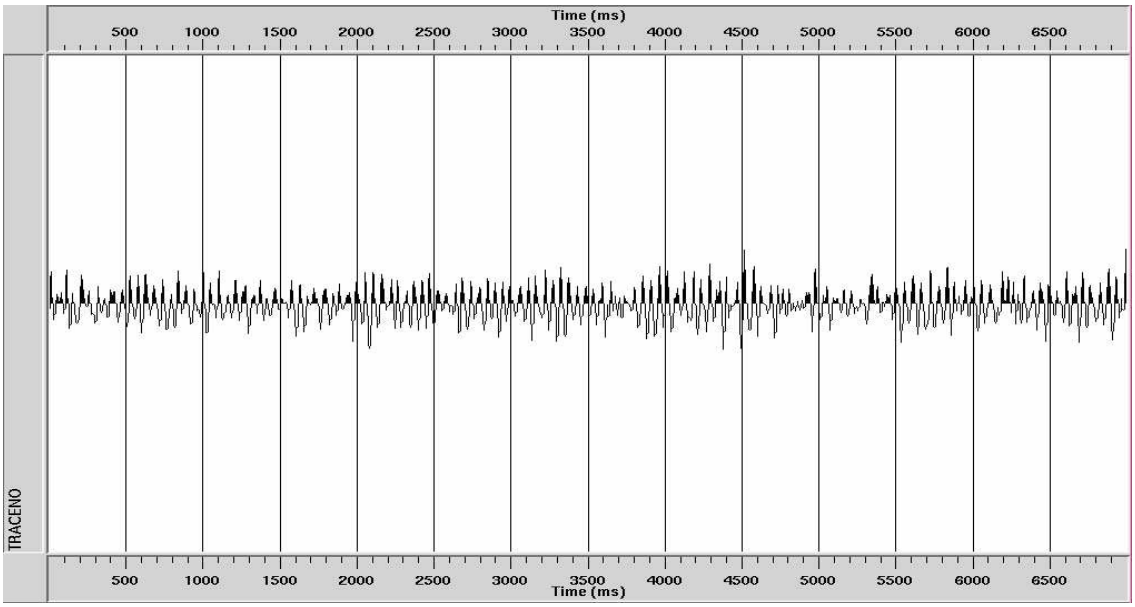

Figure 13 Raw hydrophone time trace, seven seconds long, filtered 230-250 265-285, while source is on, no signal is obvious. [The filter settings for this and other figures are given in the following manner: the reject band is at frequencies lower than the first value (in Hz) and higher than the last value. The pass band is in between the two middle frequencies. The taper from reject to pass is given (rising) by the first pair of numbers, while the taper from pass to reject is given (falling) by the second pair of numbers. In the case above, the pass band is between 250 Hz and 260 Hz.]

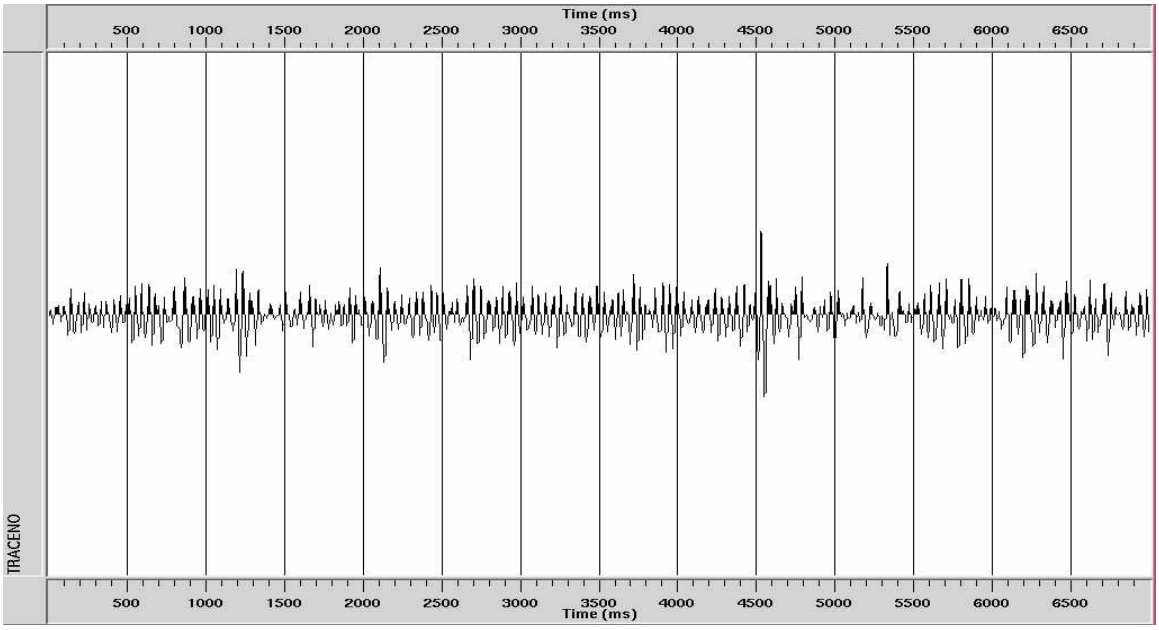

Figure 14 Raw vertical geophone time trace, seven seconds long, filtered 230—250 265-285. No signal is obvious.

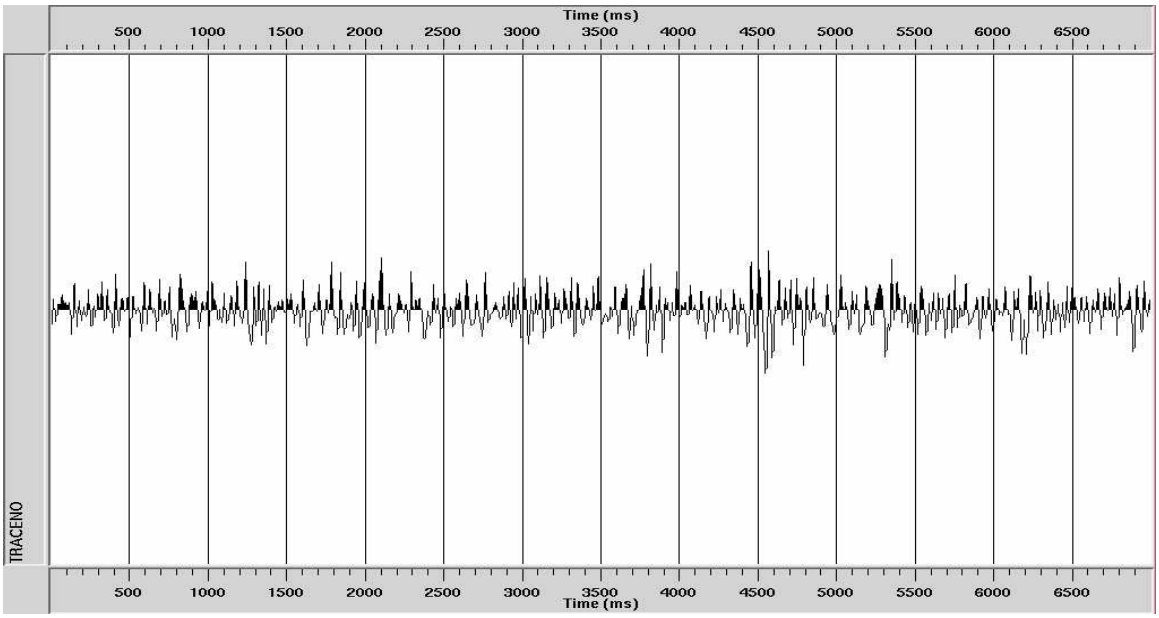

Figure 15 Raw horizontal geophone time trace, seven seconds long, filtered 230-250 265-285 while source is on, no signal is obvious

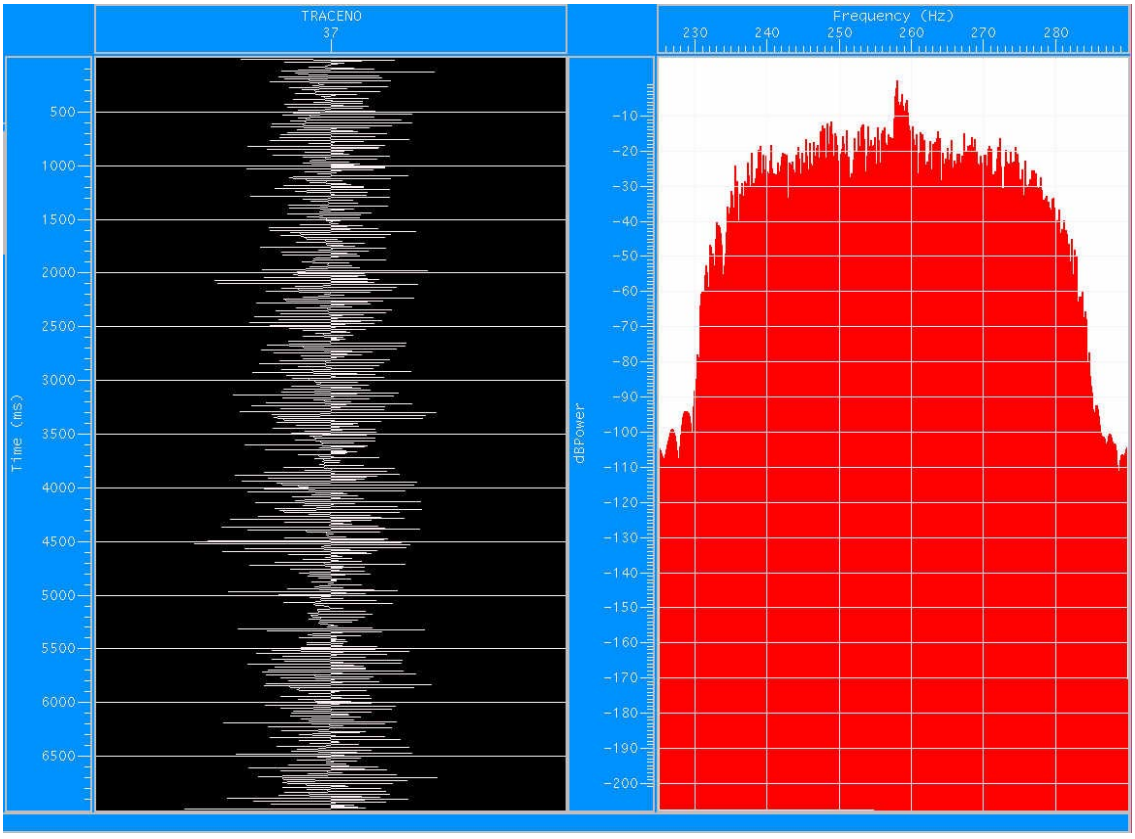

Figure 16 Time trace and spectra of the hydrophone data, filtered 230-250 265-285. The source is on, the spike in spectra at 258 Hz. is clear.

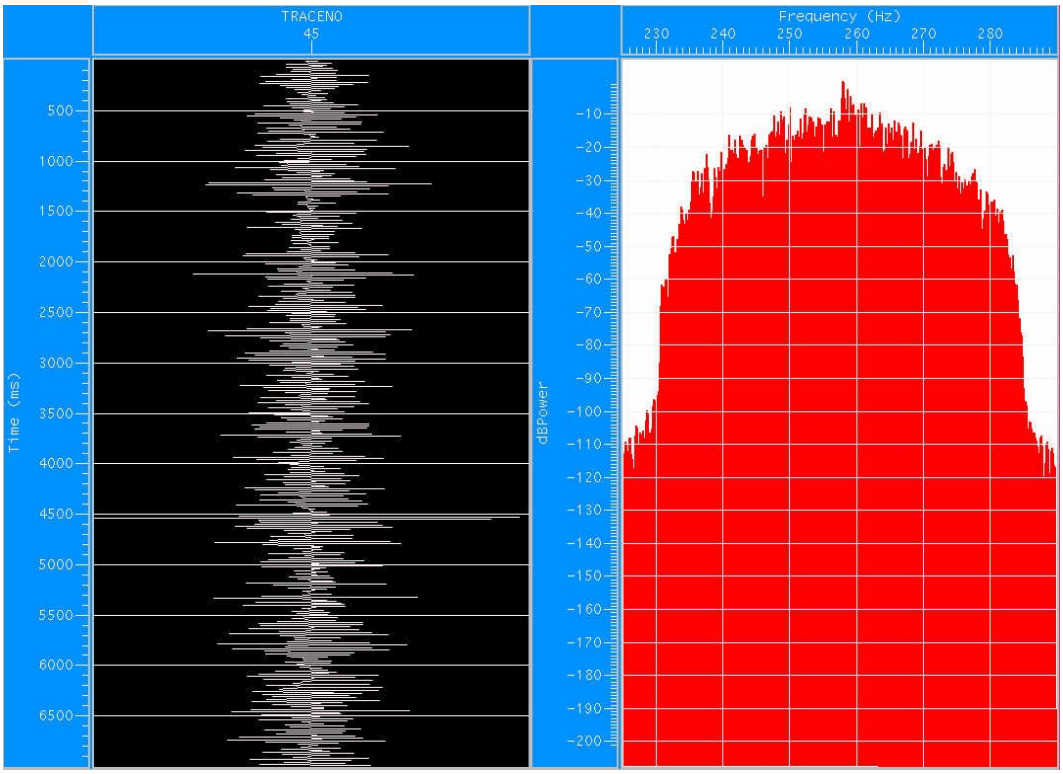

Figure 17 Spectra of the vertical geophone and associated time trace, filtered 230-250 265-285. The source is on, this is the same time period as that of the hydrophone data above. The spike at 258 Hz. is shown, not as distinct as that seen in the hydrophone data.

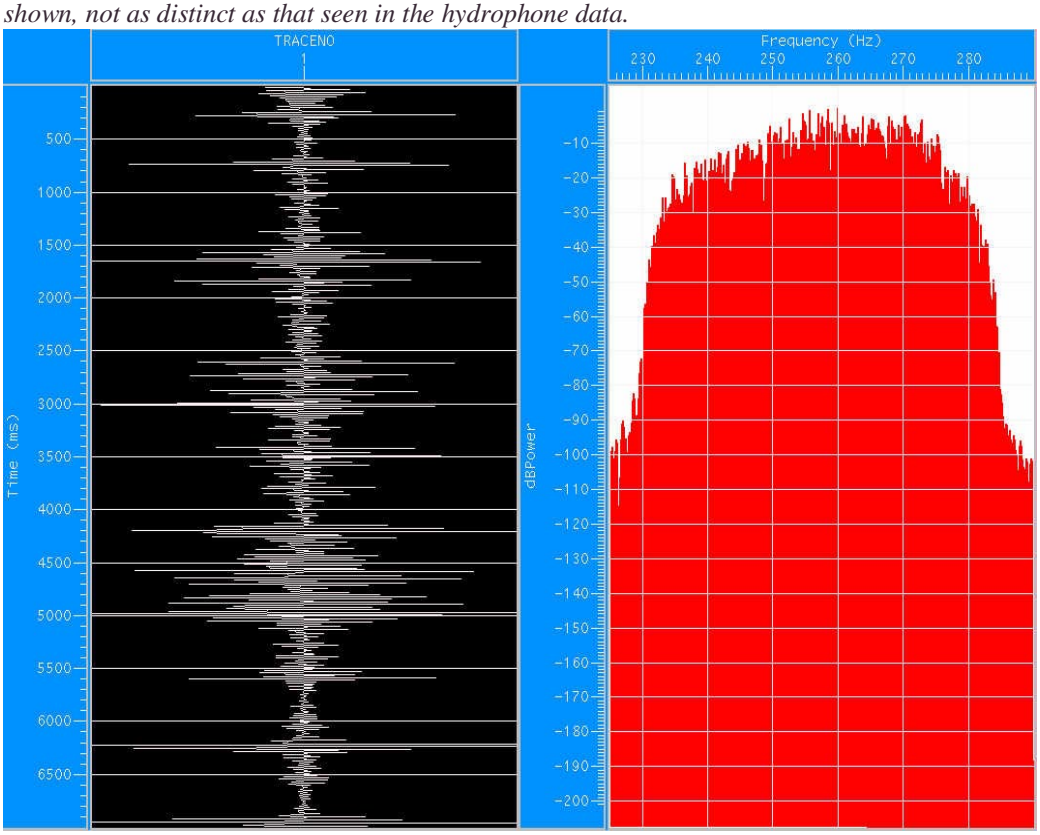

Figure 18 Noise trace, hydrophone time trace, filtered 230-250 265-285 and spectra. The source is off the spectrum is smooth.

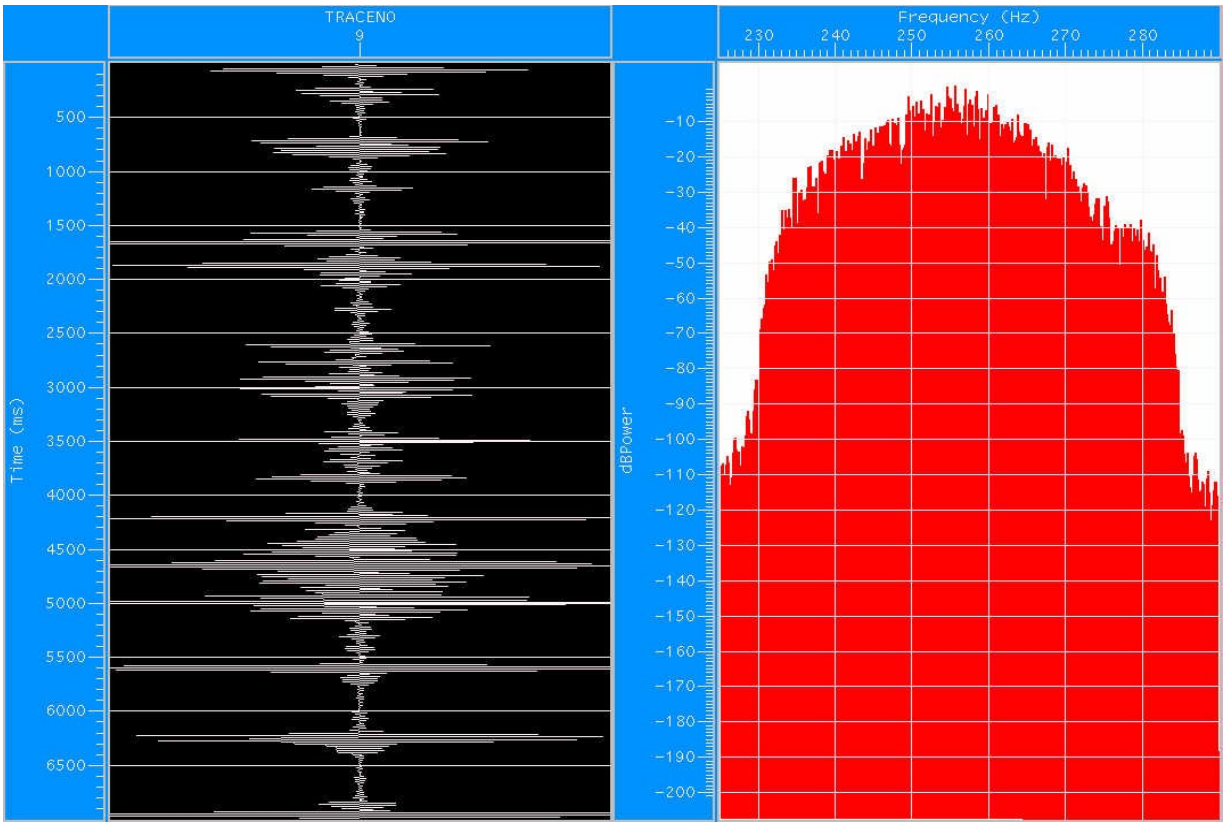

Figure 19 Noise trace vertical geophone, filtered 230-250 265-285. Spectra of a vertical geophone. The source is off, the spectrum is smooth.

Downhole Fluidics Tool

The Downhole Fluidics tool is a perforation cleaning device, deployed on tubing that emits an oscillating stream of water under high pressure. The frequency of the oscillation is controlled by splitting the downward flow of water into two streams and then redirecting those two streams such that they intersect. Downhole Fluidics deployed four different oscillator designs, i.e. four different tools, each running at different water pressure and flow rates.

Oscillator #1	2,000 psi	2.0 bbls/min
Oscillator #2	2,300 psi	1.0 bbls/min
Oscillator #3	1,300 psi	5.6 bbls/min
Oscillator #4	2,300 psi	2.0 bbls/min

This source in all three of the above configurations was operated in the MTU/Burch borehole at depths of 1,485 ft and 1,515 ft with recording system in the MTU/Stech borehole at the same depth as the source. This source is a continuous source therefore, again, seven second records were obtained when the source was operating. Prior to the operation of the source and afterwards seven second records of ambient noise were recorded.

Data

Given the nature of this source we were looking for a continuous signal of constant frequency; none was found. The spectra for all the data from all of the oscillators was compared with spectra from all of the recordings of ambient noise. We could not find a spectral peak in the data obtained when the source was on that was not also present in the ambient noise recordings. Below, we display time traces and spectra recorded during the operation of oscillator #4, believed to be the strongest signal generator.

We conclude that the signal from all four of the Downhole Fluidics Inc. sources has an amplitude level, 1,875 ft away that is less than the ambient noise level, at a depth of 1,485 ft, at our test site.

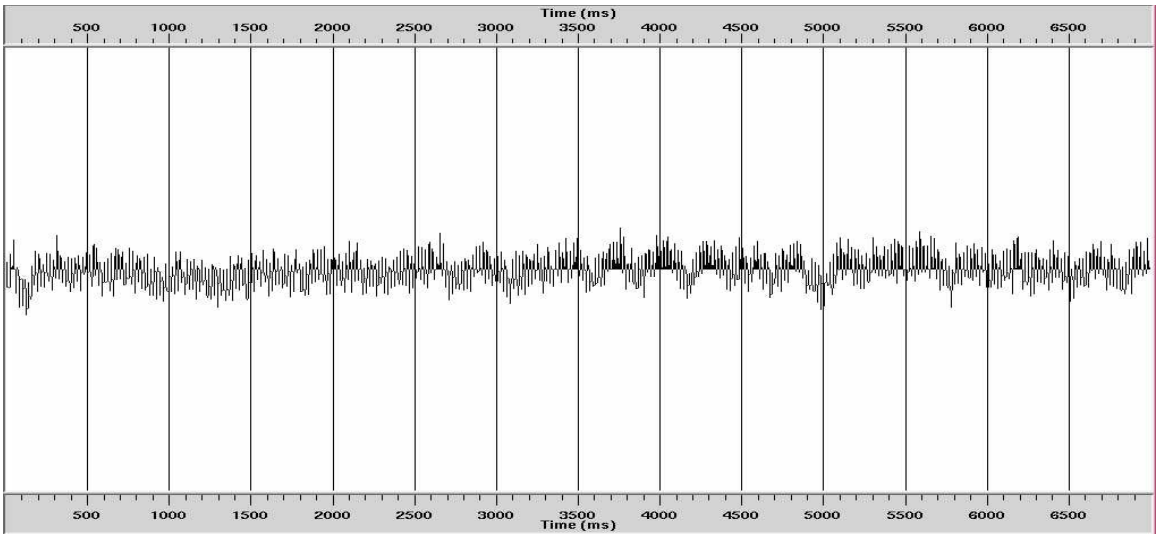

Figure 20 Raw hydrophone time trace, seven seconds long, source is on. (The apparent low-frequency signal or noise is due to aliasing of the displayed image.)

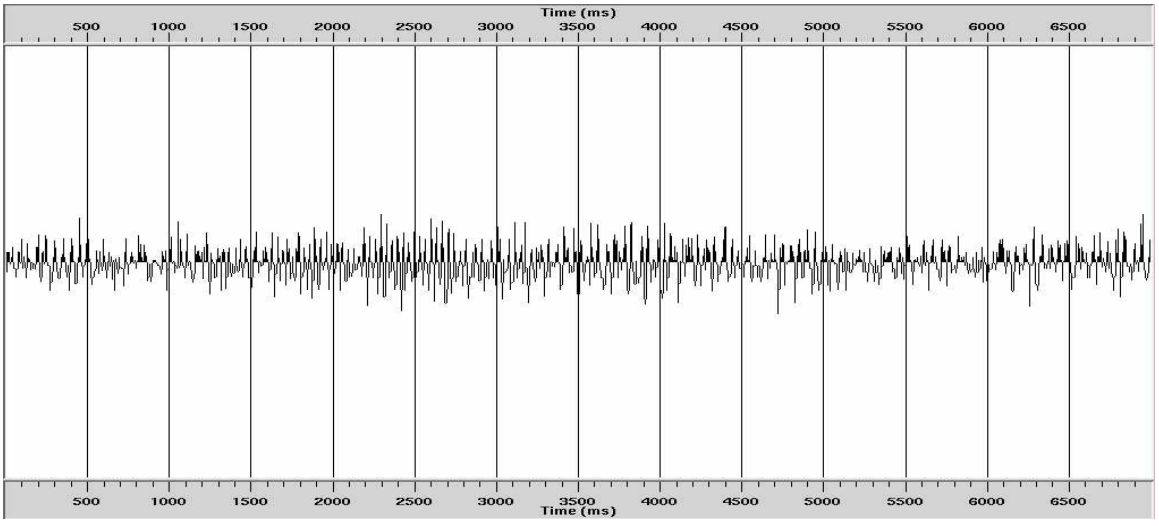

Figure 21 Raw vertical geophone time trace, seven seconds long, source is on, no signal is obvious.

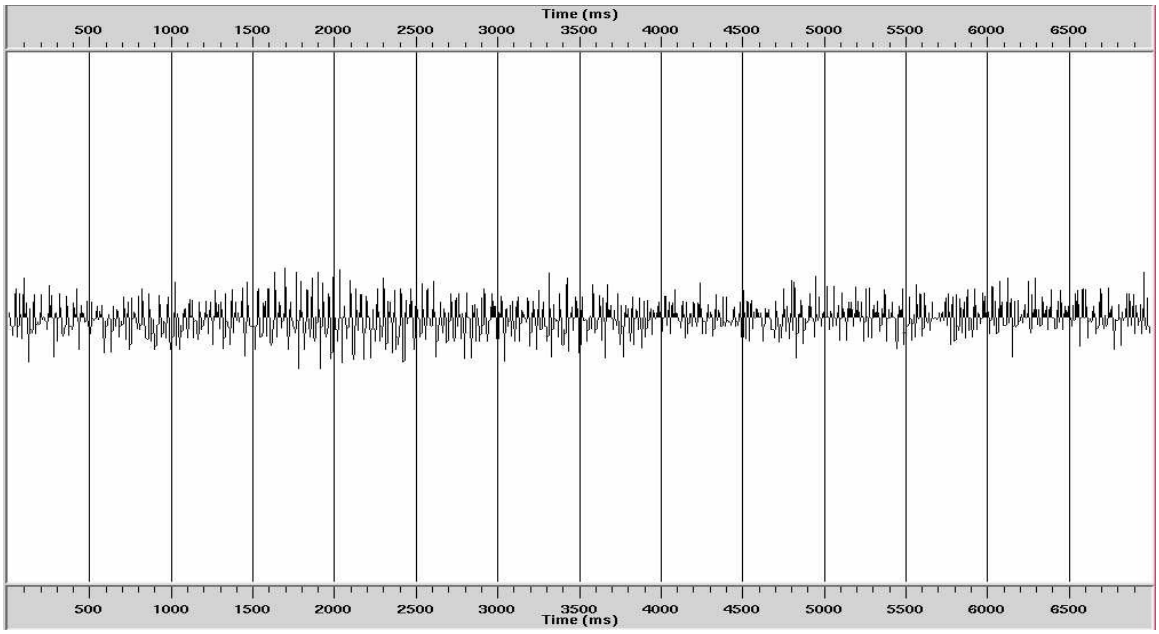

Figure 22 Raw horizontal geophone time trace, seven seconds long, source is on, no signal is obvious.

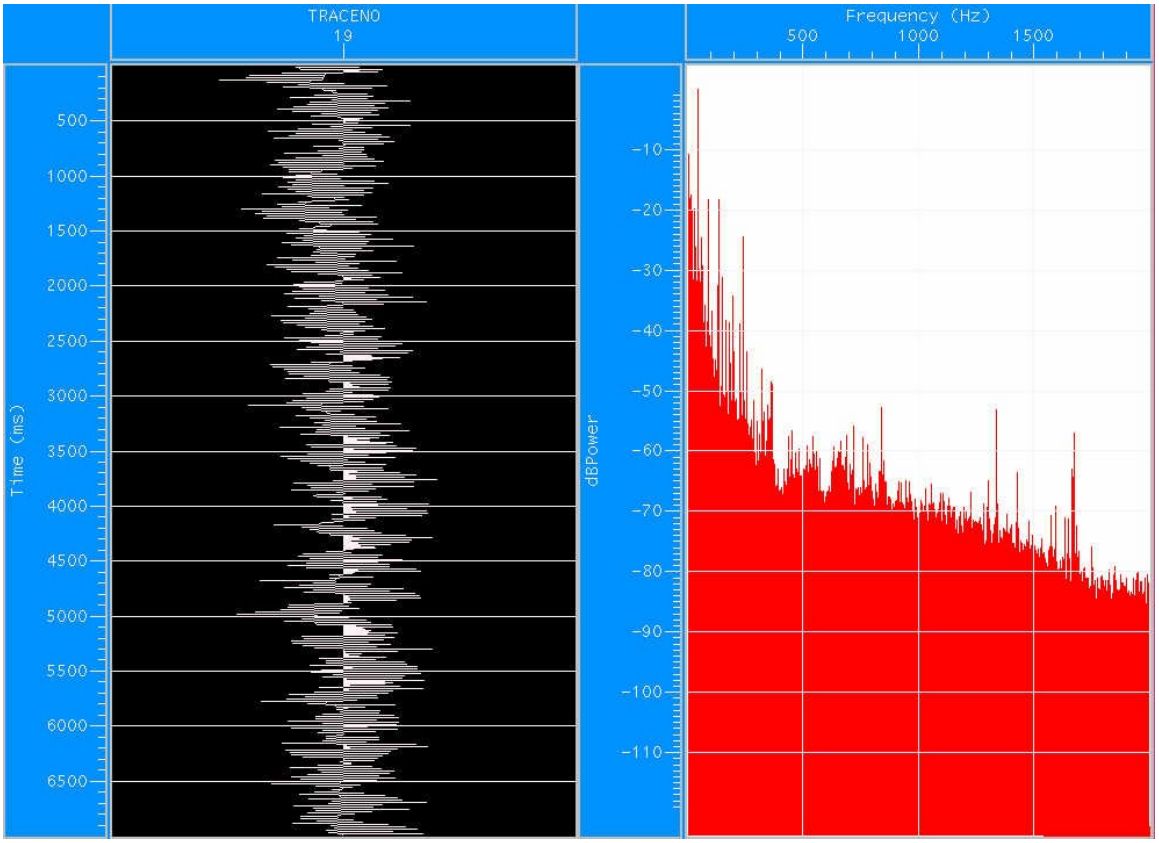

Figure 23 Spectra of the hydrophone data while the source is on, the spectra is of the entire seven second time trace shown (time trace is aliased in this display). No filtering, no signal is obvious.

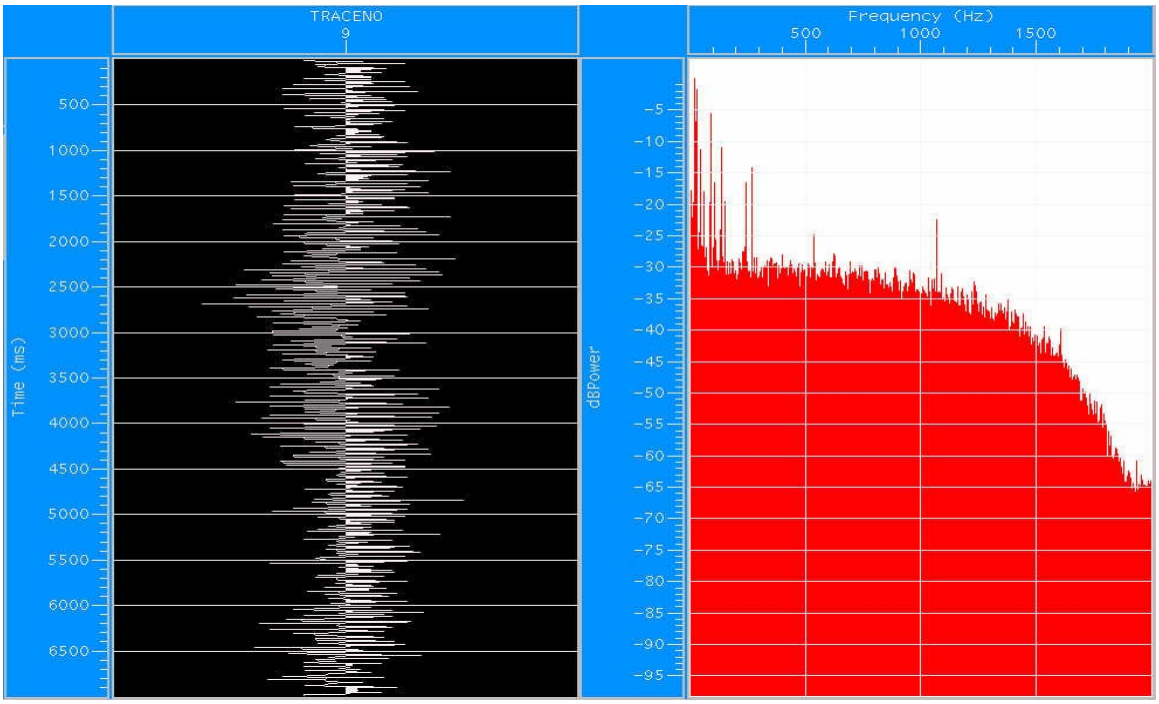

Figure 24 Spectra of the vertical geophone data while the source is on, the spectra is of the entire seven second time trace shown (time trace is aliased in this display).

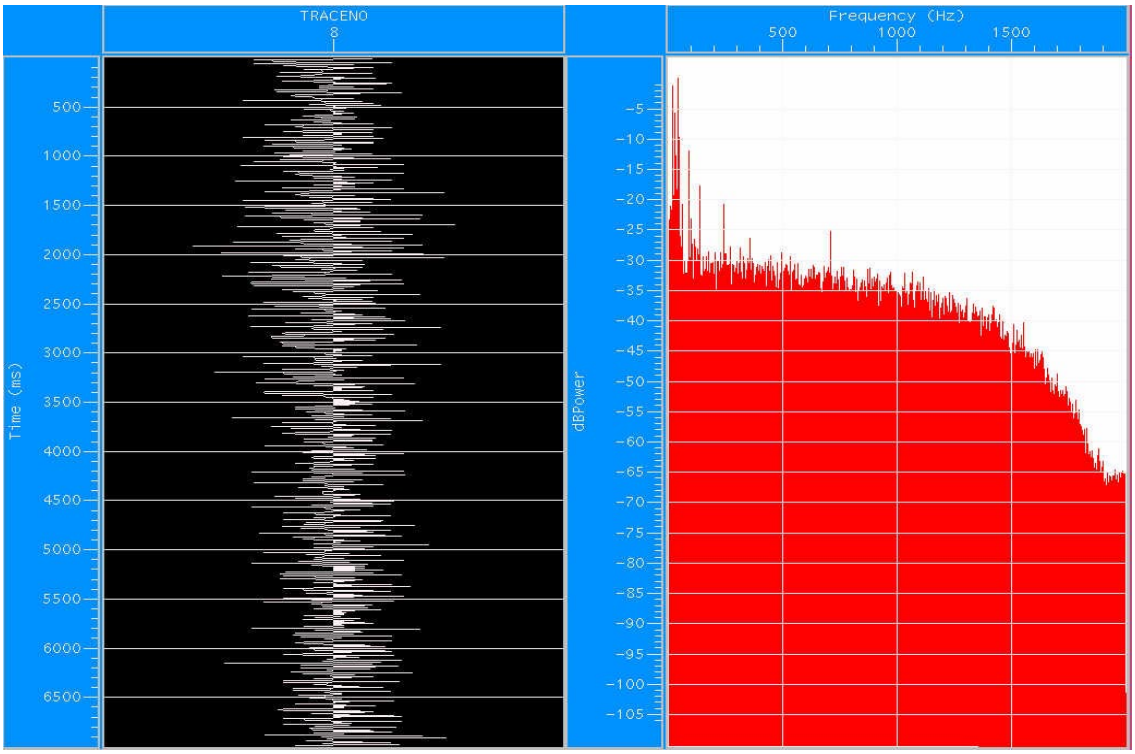

Figure 25 Spectra of the horizontal geophone data while the source is on, the spectra is of the entire seven second time trace shown (time trace is aliased in this display).

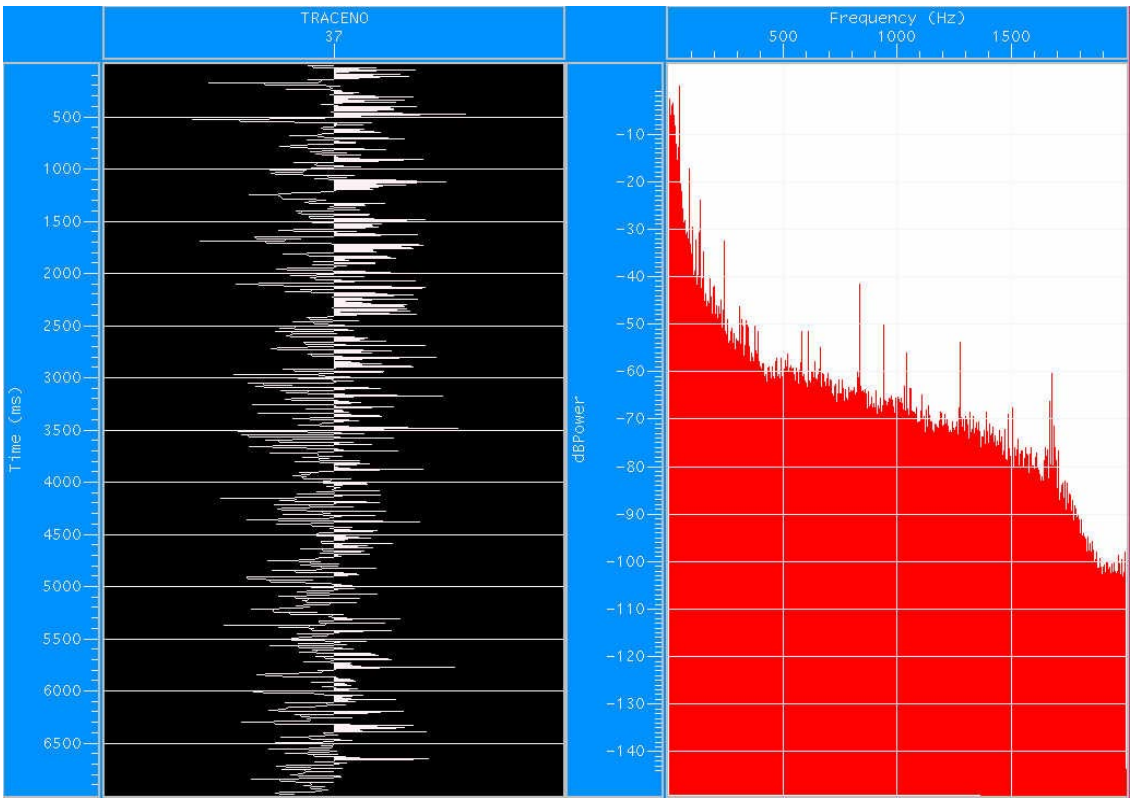

Figure 26 Spectra of the hydrophone data while the source is off, the spectra is of the entire seven second time trace shown (time trace is aliased in this display).

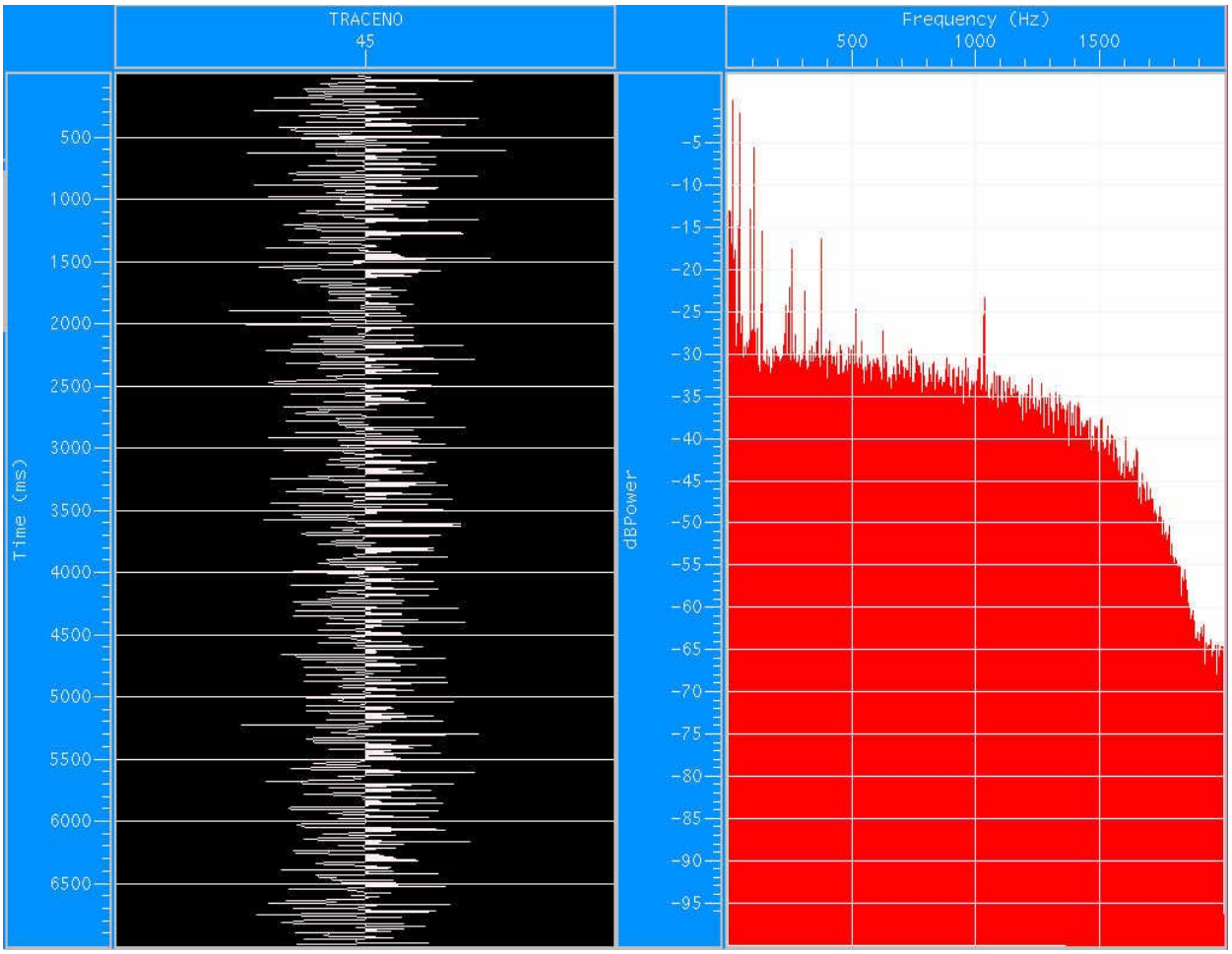

Figure 27 Noise trace and spectra, vertical geophone data while the source is off, the spectra is of the entire seven second time trace shown (time trace is aliased in this display).

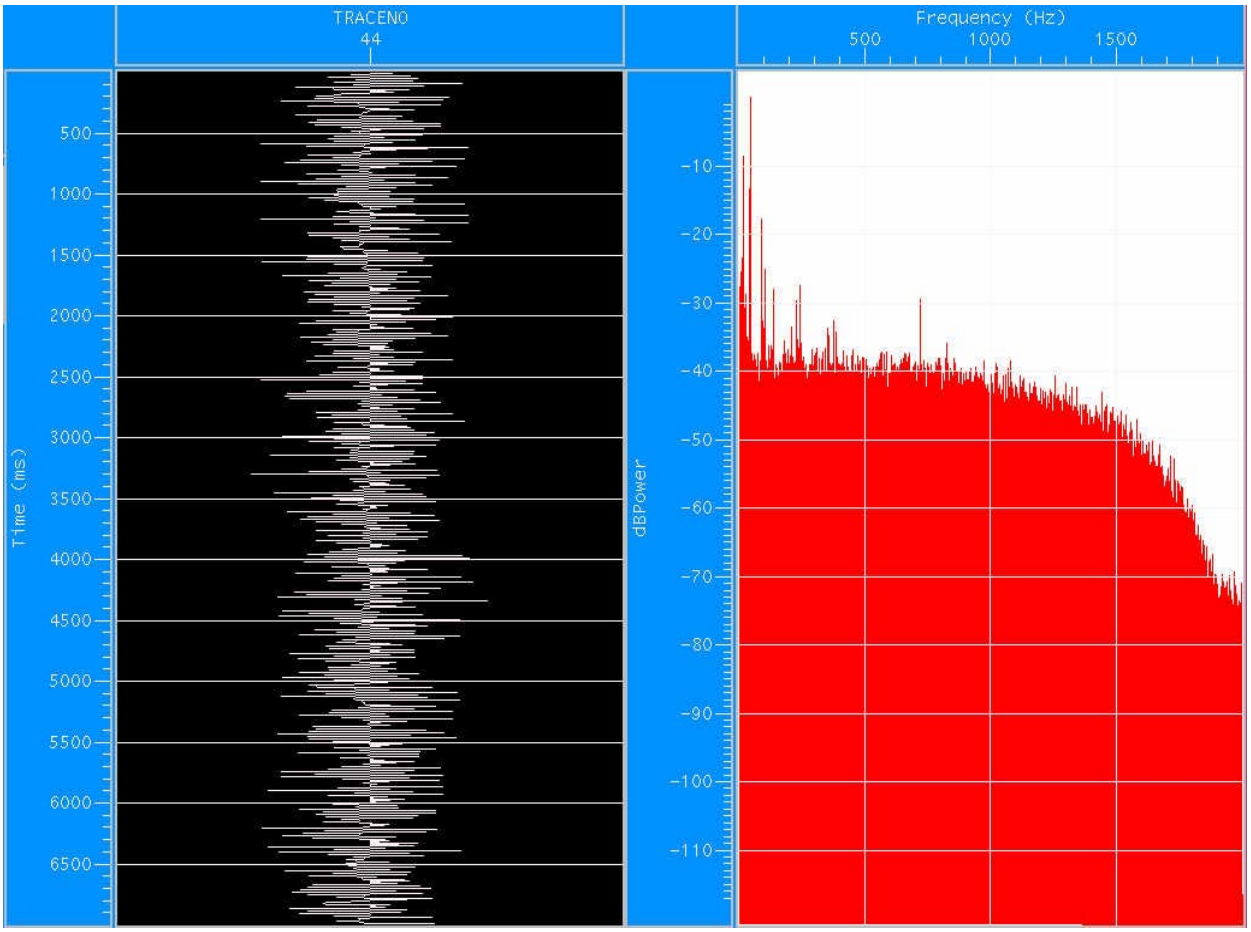

Figure 28 Spectra of the horizontal geophone data while the source is off, the spectra is of the entire seven second time trace shown (time trace is aliased in this display).

Baker Atlas Inc. Source

Baker Atlas Inc. possesses a downhole, piezo-electric source (RIS, reservoir imaging source) that was developed for seismic imaging purposes. It operates on conventional seven conductor wireline with a 850 volt signal in a frequency band from 200 Hz to 4,000 Hz. Although it can be driven by any type of signal, for this study, we chose a linear sweep, two seconds in length, from 200 to 1,600 Hz.

The upper limit of this sweep was chosen to be 1,600 Hz. because the 1/4 millisecond sampling rate (4,000 samples per second) of the recording system places the Nyquist frequency at 2,000Hz and anti-aliasing filter begins to "roll off" at 1,600Hz. (To sharply reduce the amplitude of the data at 2,000 Hz the filter begins its operation at 1,600 Hz.)

For the purposes of this study we are interested in the amplitude spectrum of a single sweep. Again, in the time traces of the hydrophone and geophone data no signal was seen, however, the spectra of both the hydrophone and geophone data clearly show the entire sweep of the source. Thus we conclude, as we have for the previous two sources, that the amplitude of one sweep is below the ambient hydrophone and geophone noise levels.

Because this source was designed for imaging purposes it is not a continuous source, it has a precise start time and the waveform driving the piezo-electric source is known. Thus, one can use conventional seismic processing procedures of correlation and stacking on these data. We used these techniques to demonstrate that indeed a signal was present at a distance of 1,875 ft.

Furthermore, we numerically modeled the seismic wave propagation for that portion of our test site using a 2-D finite-difference modeling algorithm. The resulting wave front plots (figures 7 through 11) give us the arrival time of the first signal (0.105 seconds) and of all subsequent arrivals, assuring us that the source is operating properly. A separate section of this report is devoted to the numerical modeling.

Data

The recording system and this source begin operation at the same instant with the sweep lasting, in this case, two seconds, and a listening period following that of two more seconds. Thus the raw traces are four seconds long; however, since the travel time of the first arrival is approximately one tenth of a second the strongest portion of the raw sweep arrives at the sonde during the first two seconds of that record. Moreover due to the preferential attenuation of high frequency seismic waves the strongest amplitudes will arrive in the first quarter of a second after the first arrival instant (0.350 seconds) on the hydrophone trace (because the sweep begins at 200 Hz.). However, the raw, uncorrelated hydrophone and geophone traces failed to show any signal to the naked eye. Thus, as mentioned above, we must conclude that the amplitude of a single, uncorrelated sweep is smaller than the ambient noise levels.

To demonstrate that the signal from this source was present in our data we took advantage of stacking and correlation, the conventional seismic processing tools. As shown below, after stacking ten correlated traces we obtained a very clear signal on both the hydrophone and geophones. In fact, the strongest first arrival on the geophone package was on a horizontal geophone just as the numerical modeling suggests. Furthermore, the excellent data obtained here has allowed us to update our velocity model for the test site. We now know that the Traverse Limestone exhibits anisotropy with the horizontal compressional wave velocity being 17,860 ft/sec while the velocity for vertically propagating compressional waves is 18,200 ft/sec

To be consistent with the previous sources we display data acquired at a depth of 1,485 ft with the source in the MTU/Stech borehole and the receivers in the MTU/Burch borehole.

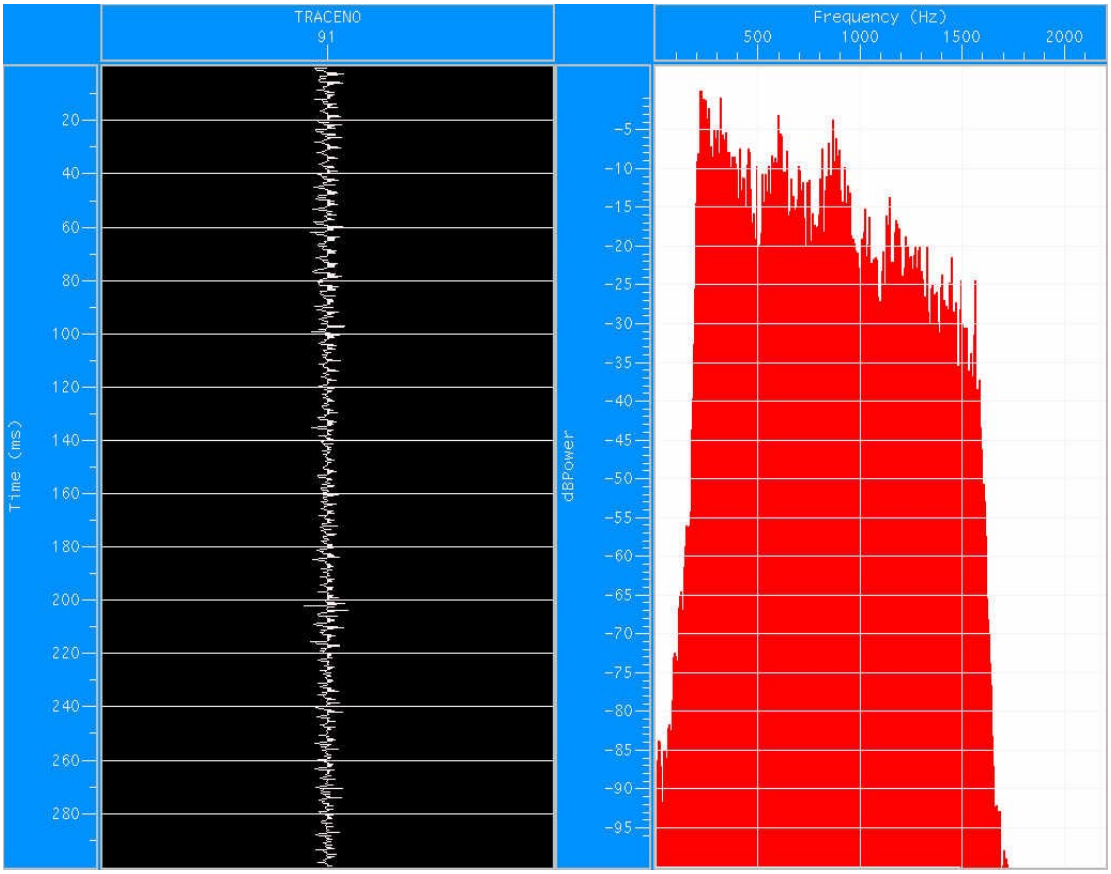

Figure 29 Raw, uncorrelated hydrophone time trace and spectra, source is operating, filtered 180-200 1600-1620, no signal is obvious. Sweep should start at approx. 0.1 seconds.

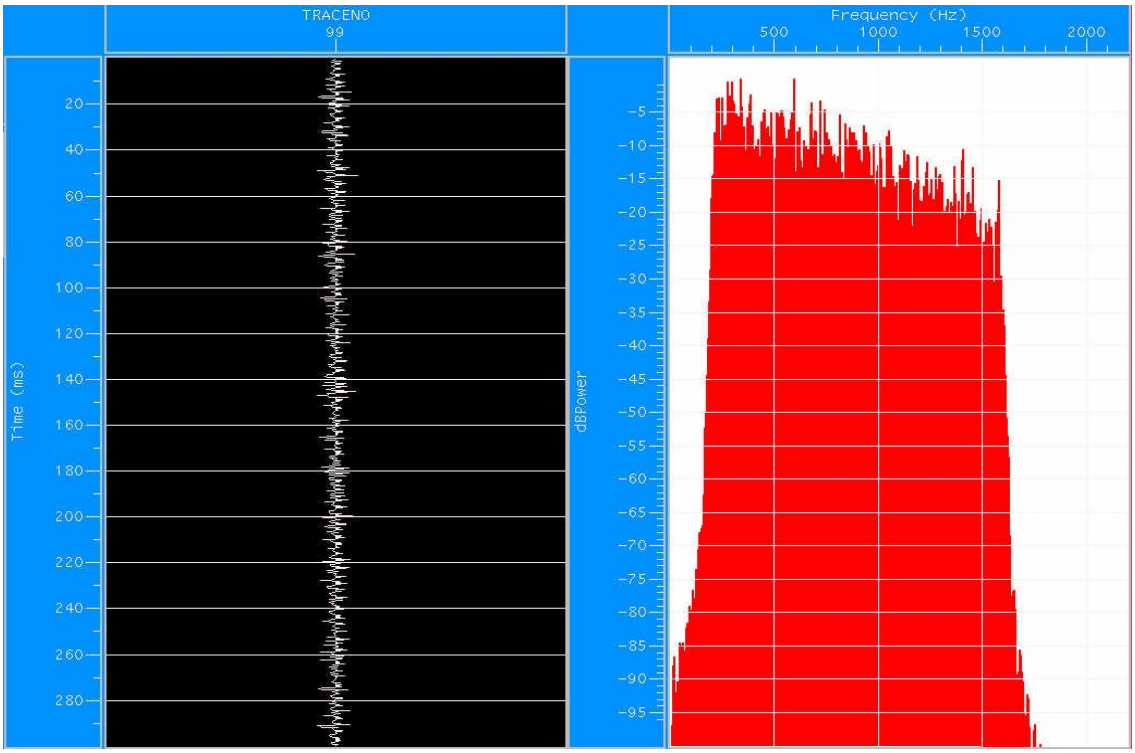

Figure 30 Raw, uncorrelated vertical geophone time trace and spectra, source is operating, filtered 180-200 1600-1620. Even though the data has been filtered in the band of the sweep no signal is obvious.

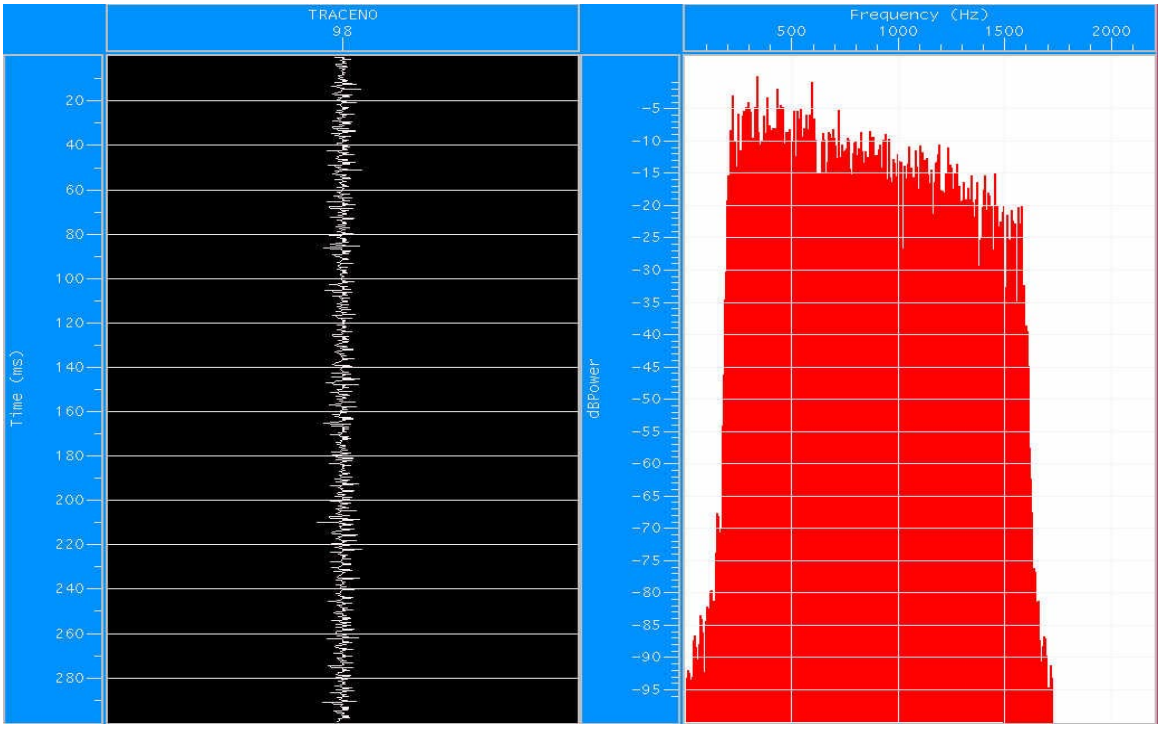

Figure 31 Raw, uncorrelated horizontal geophone time trace and spectra, source is operating, filtered 180-200 1600-1620

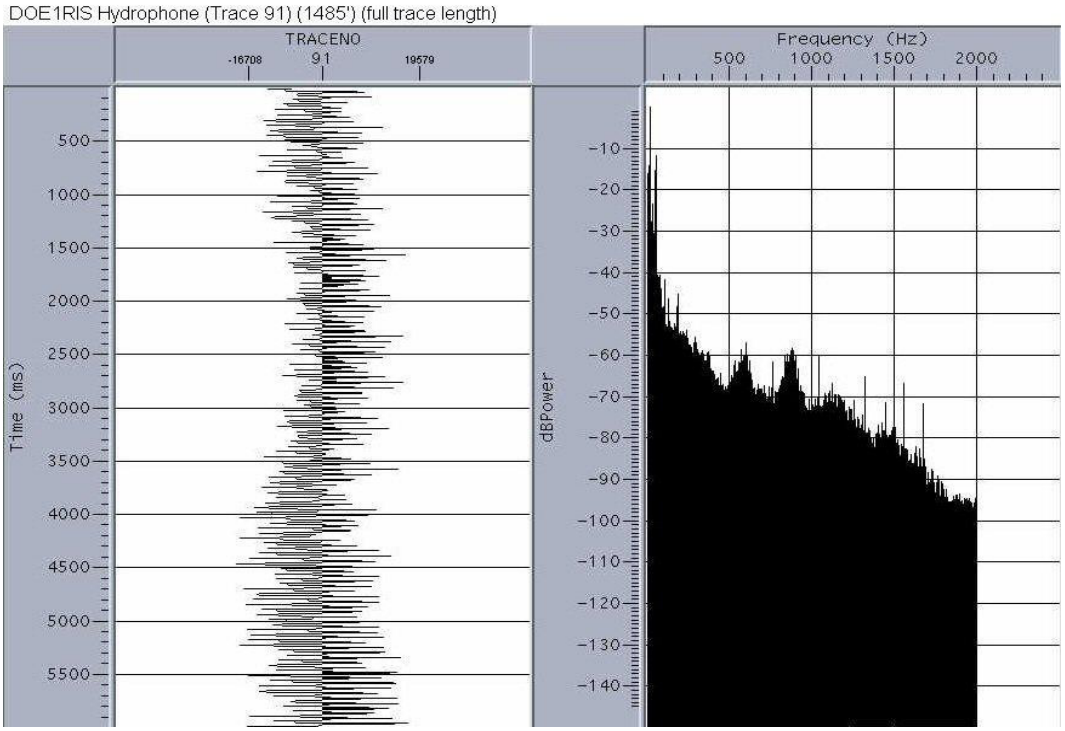

Figure 32 Six second noise trace, hydrophone, source is not operating.

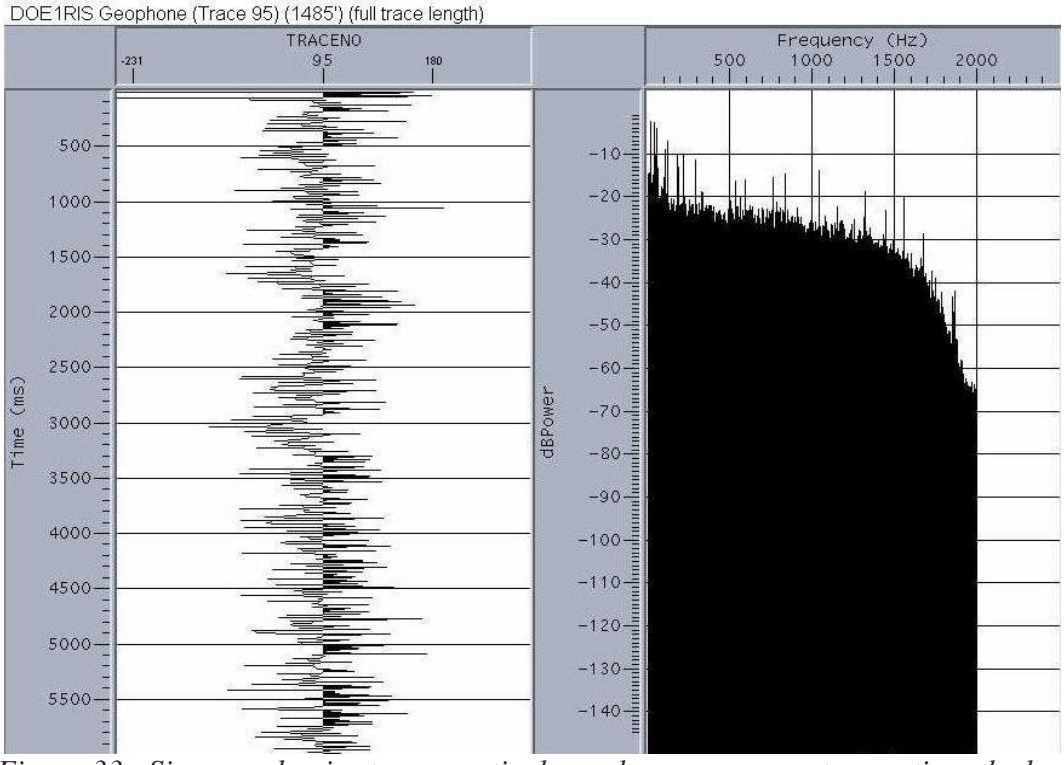

Figure 33 Six second noise trace, vertical geophone, source not operating, the knee in the spectrum at 1,600 Hz is the system's anti-aliasing filter.

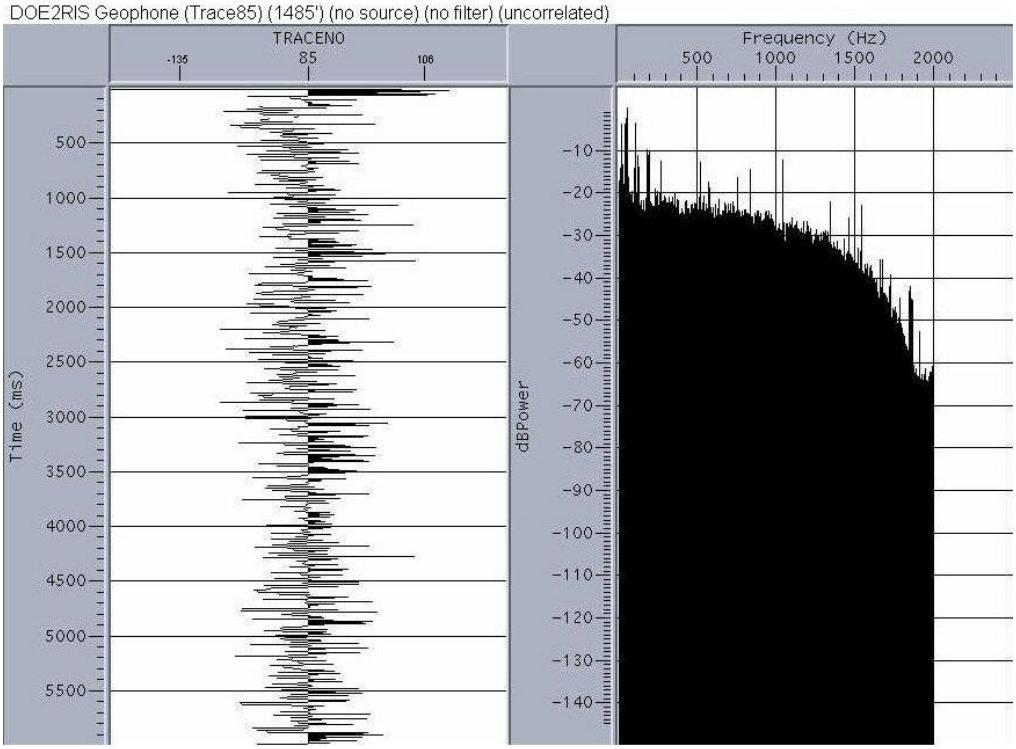

Figure 34 Six second noise trace, horizontal geophone, the source is not operating. The knee in the spectrum at 1,600 Hz is the anti-aliasing filter.

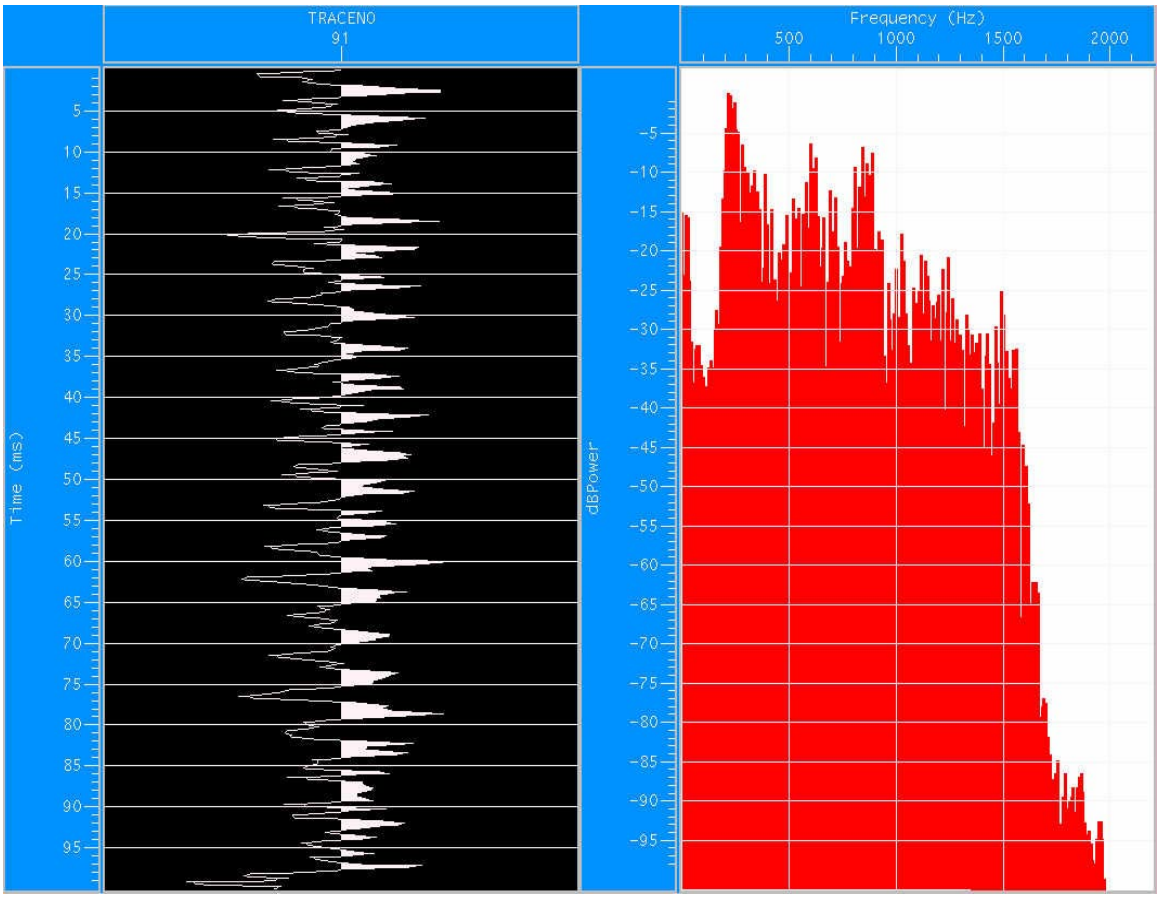

Figure 35 Ambient noise, hydrophone time trace (not aliased) and spectrum, prior to signal arrival.

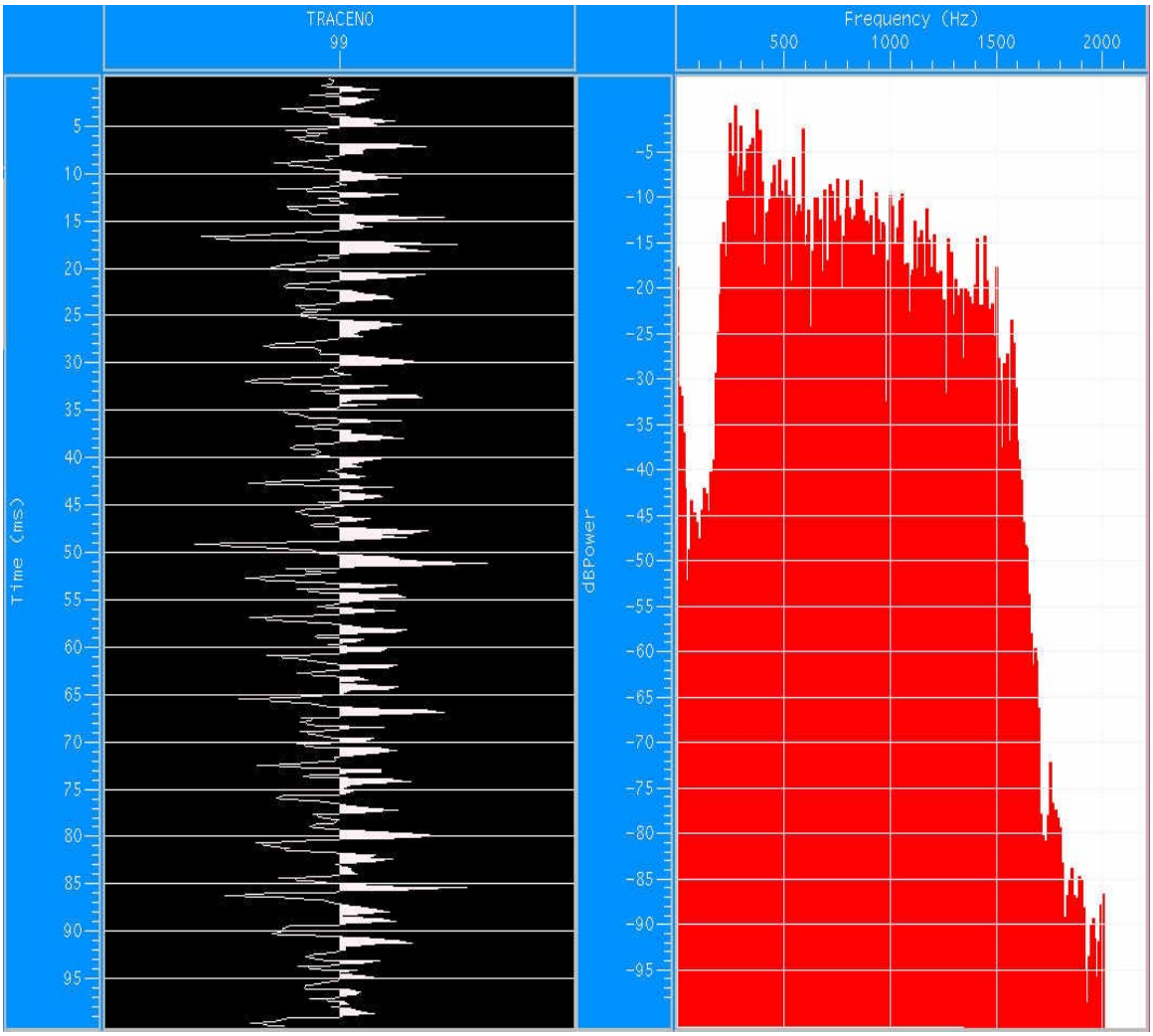

Figure 36 Ambient noise, vertical geophone time trace and spectra, prior to signal arrival

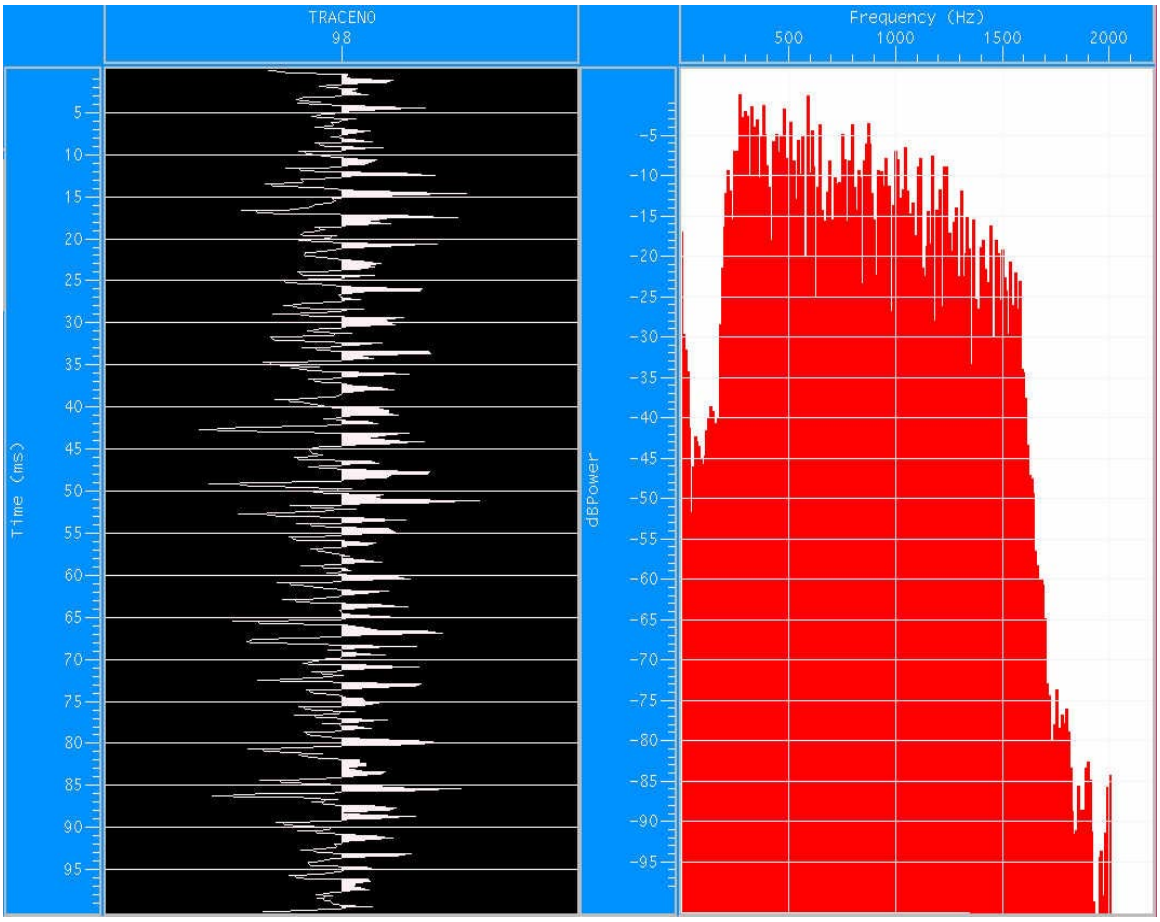

Figure 37 Ambient noise, horizontal geophone time trace and spectra, prior to signal arrival

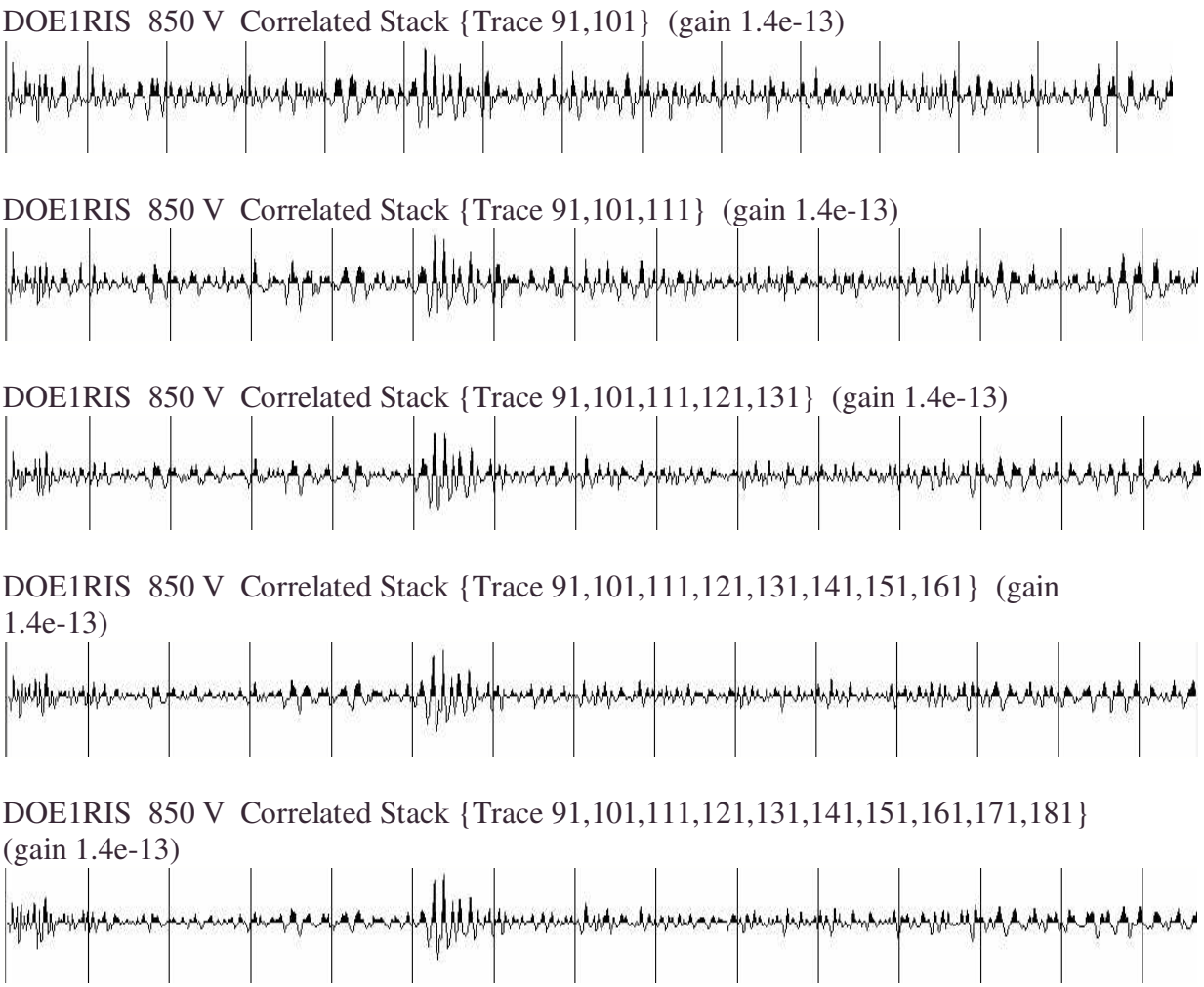

Figure 38 Display of sequential stacking of the ten correlated hydrophone traces, S/N improves, as expected, as each trace is added to the stack. This data demonstrates the existence of a signal and the fact that its arrival time corresponds to that seen in the numerical modeling.

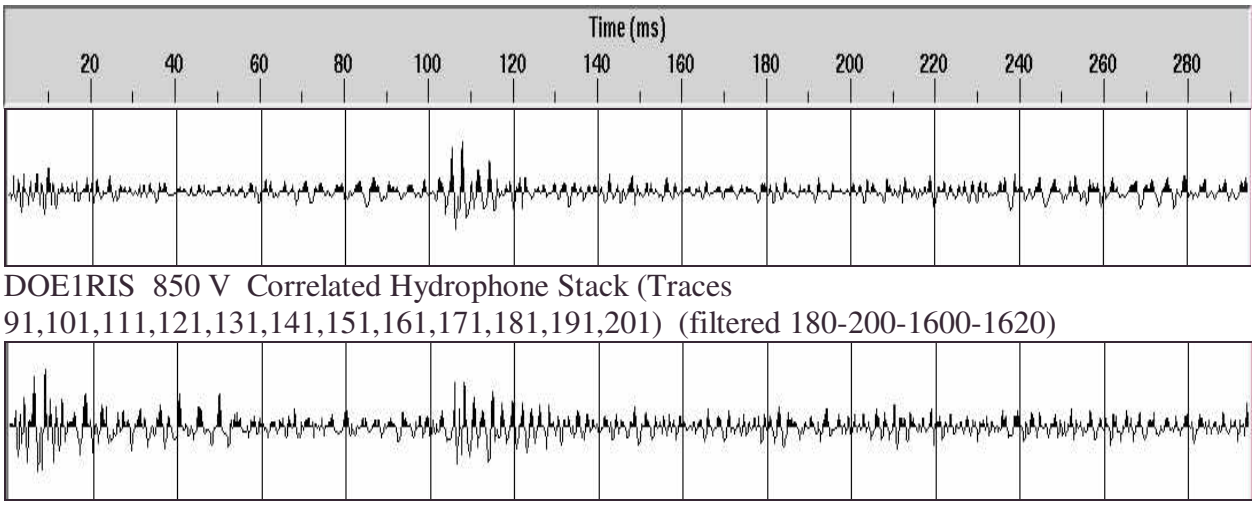

Figure 39 Comparison of stack of ten hydrophone traces and stack of ten, horizontal geophone traces (lower trace). Here we demonstrate the fact that the signal is clearly seen on both hydrophone and geophone traces and in particular a horizontal geophone trace as would be expected from the geometry of the test.

Industrial Vehicles International Inc.
Surface Vibrator

The mid-program review workshop, held in Tulsa, Okla. on June 15, 2004 strongly suggested that we include a surface vibrator in our second data acquisition session. Bay Geophysical Associates Inc. provided an IVI truck mounted vertical vibrator that produced 6,000 lbs of force.

The vibrator was placed 774 ft away from the MTU/Stech and the receiver sonde was clamped at 1,485 ft. We chose a 10-second linear sweep from 18Hz to 360Hz with 2 seconds of listen time. This source is strong enough that a single, uncorrelated sweep is visible on all sensors. The strongest portion of that sweep is in the 35 Hz region of the sweep, i.e. approximately one second into the sweep. Several sweeps were recorded. For this report six correlated sweeps were stacked yielding excellent seismic traces. The arrival times of various events fit with our knowledge of the test site.

Data
Because of the low frequency nature of this source the geophones recorded this source much better than the hydrophones. The vibrator was deployed on the surface therefore approximately 600 ft of the 1,675 ft ray path was spent in the glacial till. The IVI vibrator was strong enough that one can see the onset of a single, uncorrelated sweep on all sensors; however, we can not see the entire sweep with the naked eye. At a point less than halfway through the sweep (4.7 seconds, i.e. as the sweep reaches 160 Hz) the signal disappears into the ambient noise. Furthermore, the entire spectrum of a single, uncorrelated sweep is not seen. However at about 35 Hz, we see signal amplitudes on the vertical geophone that are approximately 20 times greater than ambient noise levels, i.e. approximately 4.5×10^{-5} cm/sec.

Stacks of correlated sweeps display clear seismic traces with high signal-to-noise. Although we have no interest in these data for sonic stimulation applications, they do provide the travel time of the first arrivals (0.31 seconds) and subsequent arrivals. We also see that the predominant frequency of the first arrival is approximately 100 Hz.

Even the spectra of correlated and stacked traces continue to show a lack of high frequencies with 160 Hz being the upper limit.

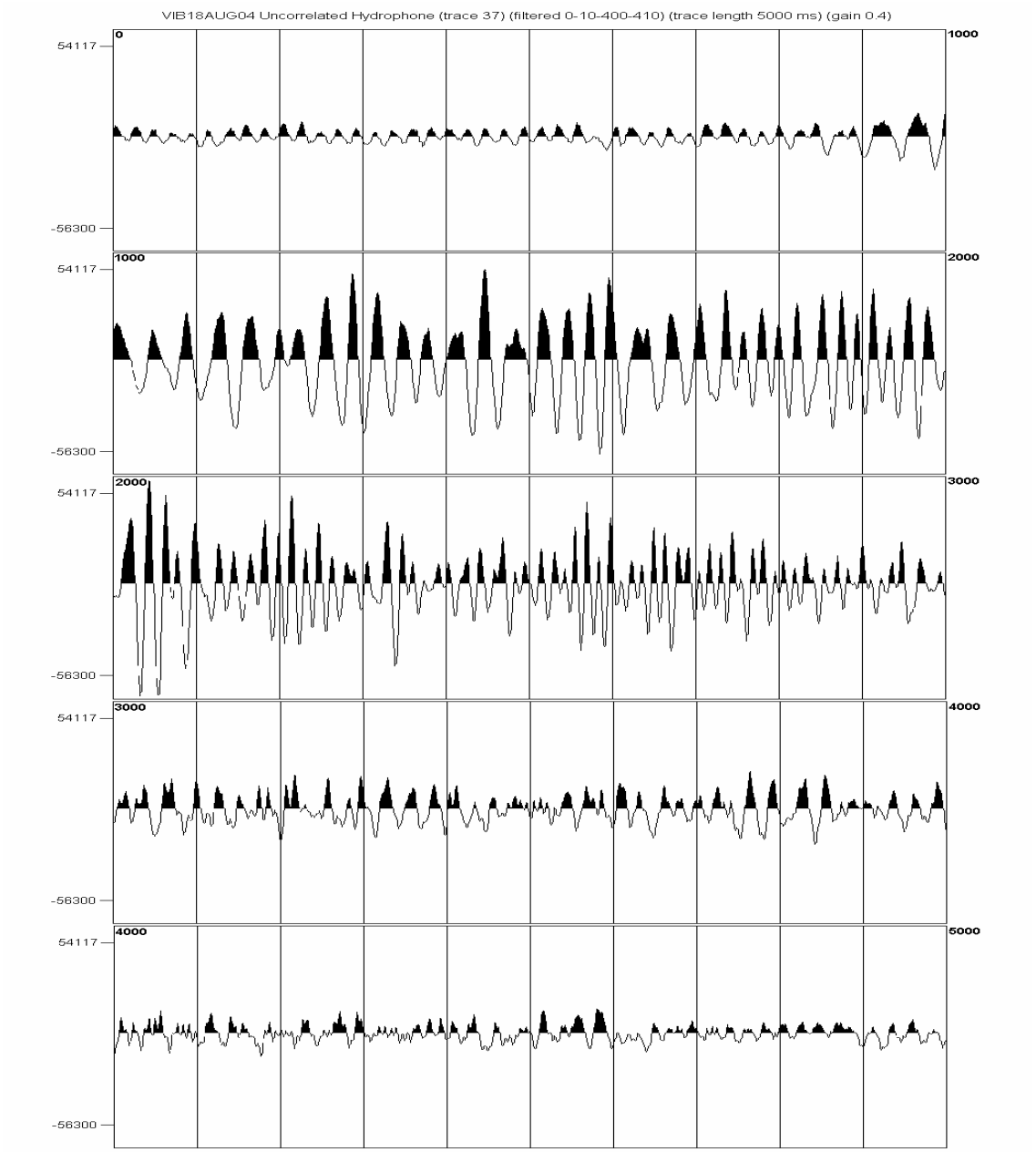

Figure 40 Single, uncorrelated sweep as seen on a hydrophone at a depth of 1,485ft. At this depth the sweep arrives at approximately 0.3 seconds and the peak occurs at 2.05 seconds.

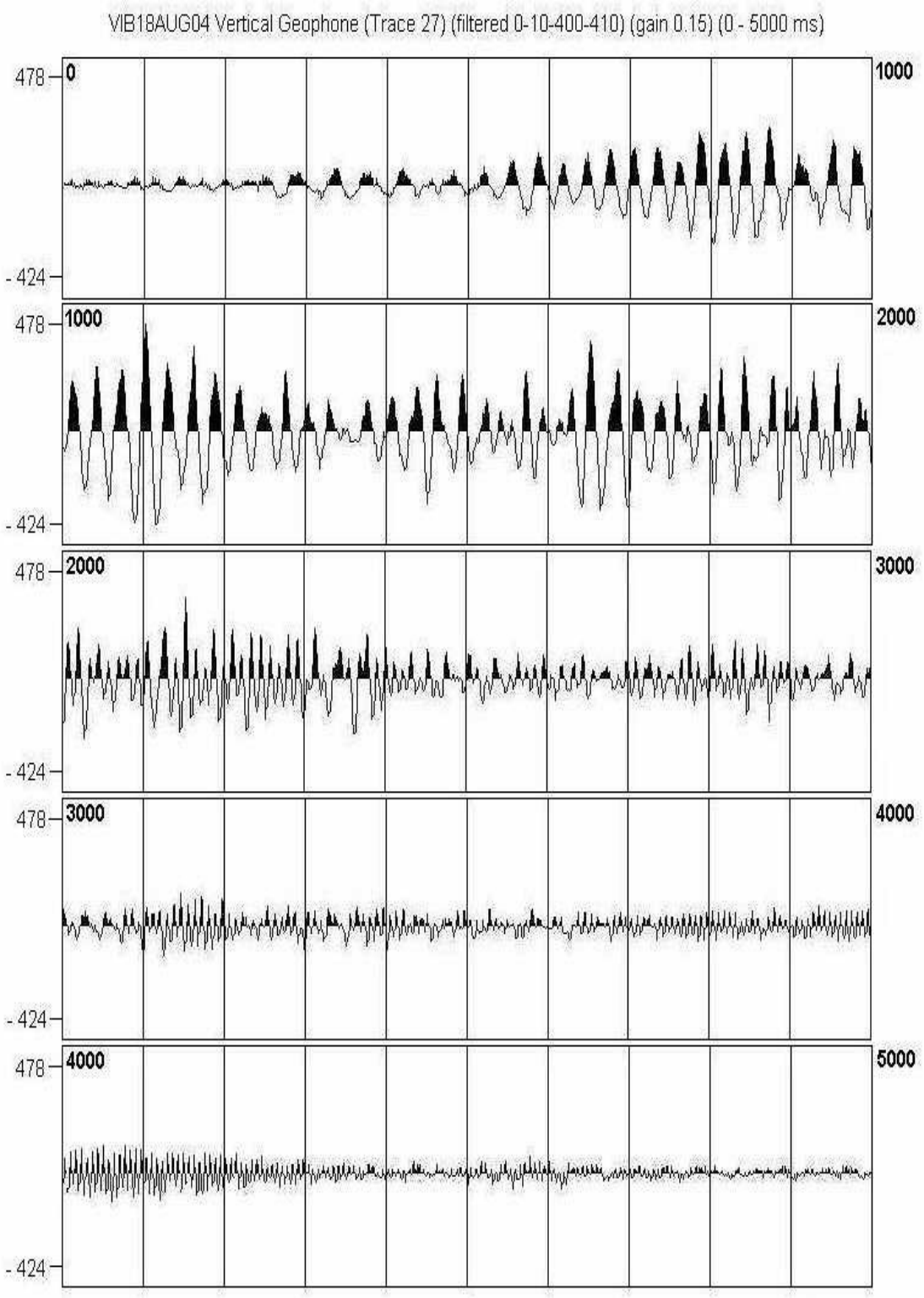

Figure 41 Single, uncorrelated sweep as seen on a vertical geophone. Note that the signal is strongest at approx. 1.1 seconds at roughly 35 Hz. The amplitude at that point is approximately 4.5 X 10^{-5} cm/sec.

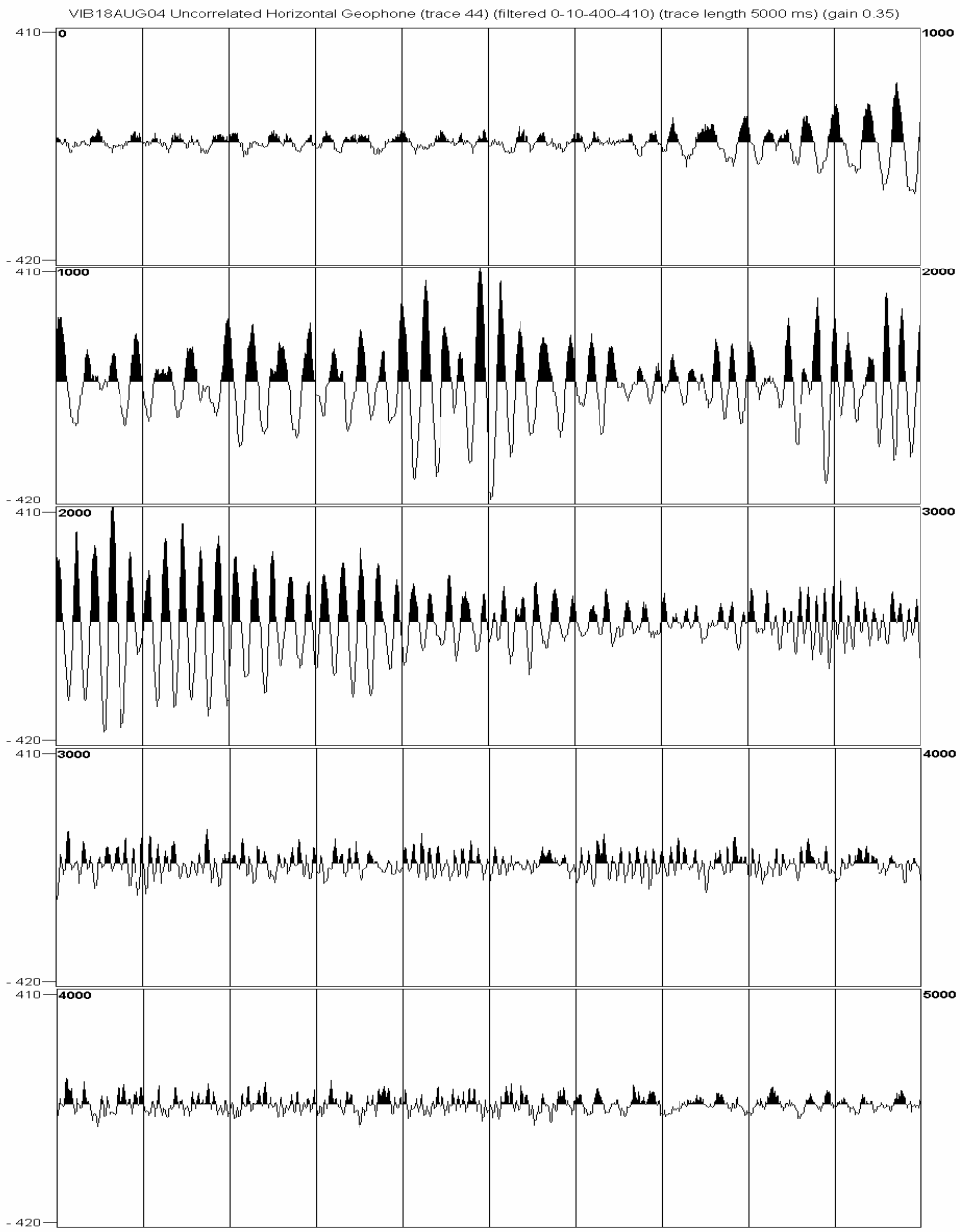

Figure 42 Single, uncorrelated sweep as seen on a horizontal geophone. Here the sweep peaks at approx. 1.5 seconds

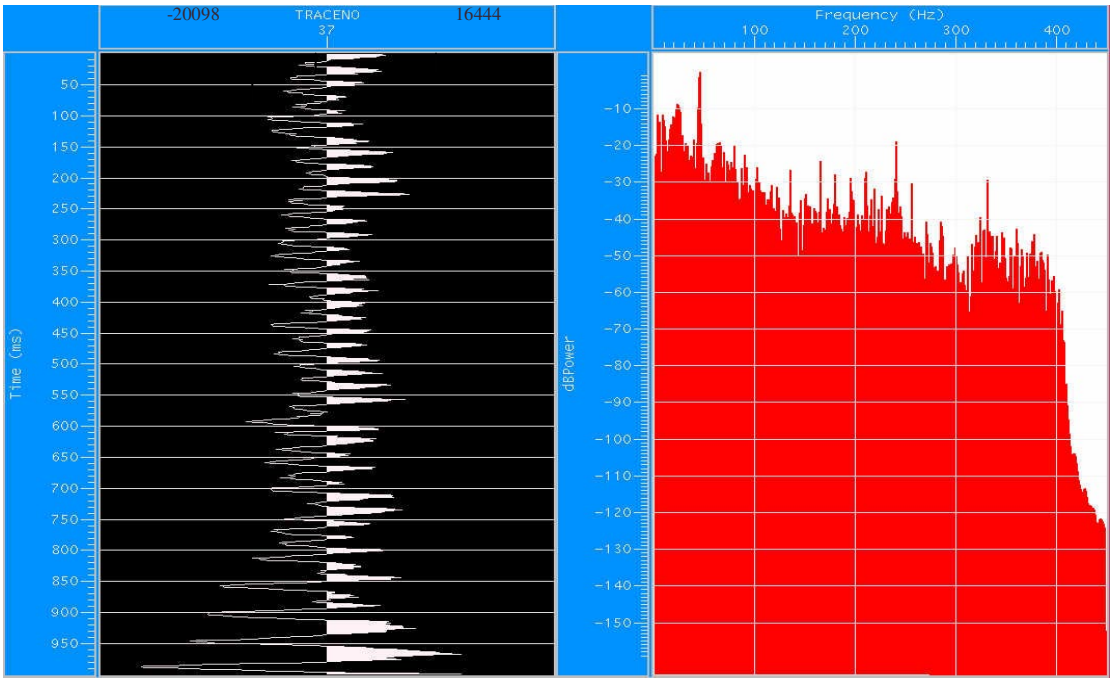

Figure 44 Spectrum and associated trace of single, uncorrelated sweep as seen on a hydrophone, filtered 0-10 400-410

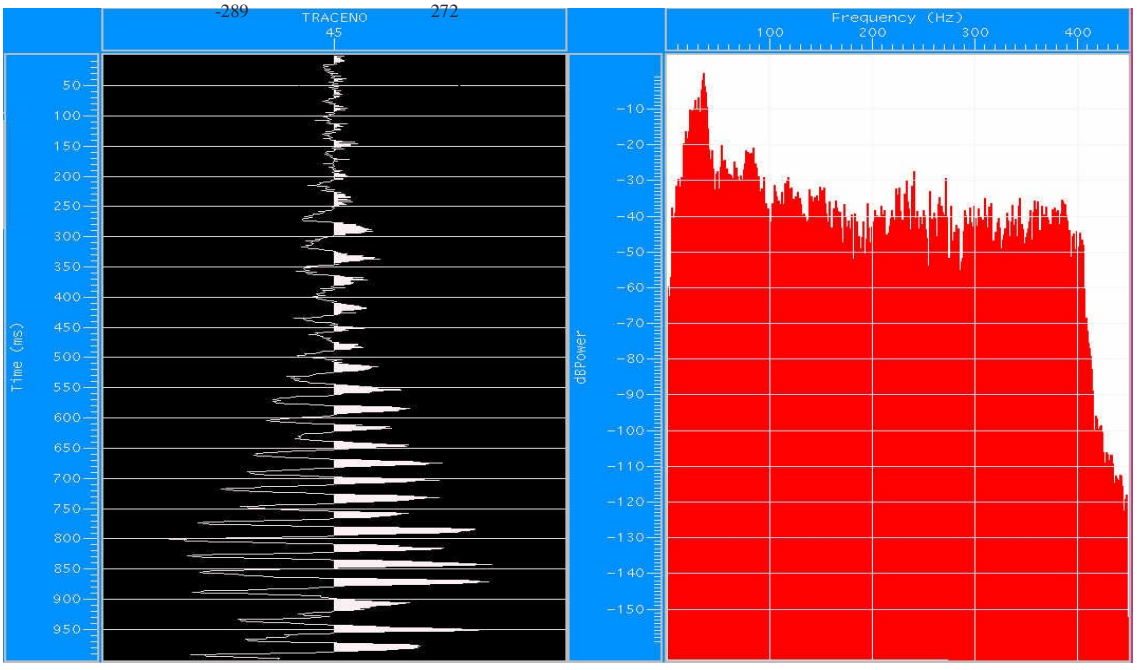

Figure 45 Spectrum and associated trace of single, uncorrelated sweep as seen on a vertical geophone filtered 0-10 400-410

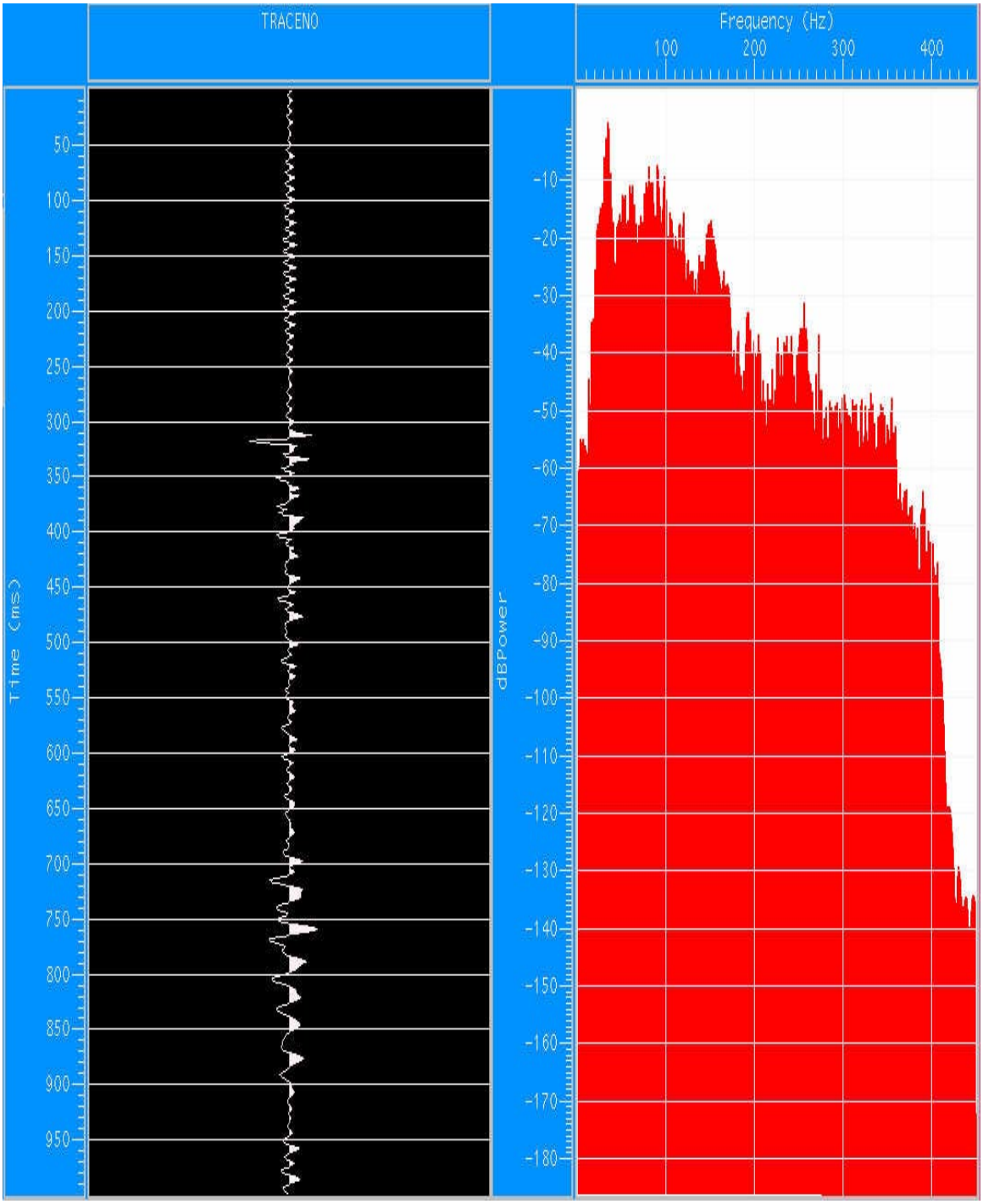

Figure 47 Vertical geophone trace of a stack of six correlated sweeps, filtered 0-10 400-410. Note that even though we have stacked six sweeps the signal is 40db down at 180Hz. We use this clear signal to identify the correct arrival time for a surface source (offset from the recording well) shooting into the receiver at 1,485ft.

Discussion of Data

A single activation of each of the three downhole sources was not strong enough to be seen on the time traces of either the geophones or the hydrophones. However, in the case of the Clean Wells source we believe that the spectra of both the hydrophones and the vertical geophones showed a signal (258 Hz) from the source. Given the physical operation of the Clean Wells source (fluid flow from an oscillating nozzle) a continuous signal is expected. We examined the ambient noise records acquired during the recording of the Clean Wells source and found no similar spike in the spectra. We narrowly band-filtered both the ambient noise data and the data acquired while the source was on; a clear spike was found in the data taken while the source was on and no spike while the source was off (ambient noise). Thus we conclude that the signal amplitude from the Clean Wells source is below the ambient noise level.

The Downhole Fluidics source should also produce a continuous signal (fluid flow from two nozzle but none was detected either on the time traces or in the spectra. We have to conclude that the signal amplitude from this source also is below the ambient noise level.

The signal from Baker Atlas's piezo-electric source was designed for seismic imaging, therefore it can be driven by a known function, starting at a known time. However, in this study we were interested in the signal level of one activation of the source and on the geophone and hydrophone time traces we could find no signal. Thus we conclude that the signal amplitude is less than the ambient noise level.

To show that, indeed, a signal did exist during our data acquisition periods we correlated hydrophone and geophone records with the known sweep (2 seconds long, 200 Hz to 1,600 Hz). After correlation a single sweep was seen on the hydrophone data and on the horizontal geophone data. After stacking ten such hydrophone records and ten horizontal geophone records we obtained signals that would be termed excellent for seismic imaging purposes.

Thus for the three downhole sources we can only say that their signal levels are below the ambient noise levels 1,485 ft below the surface in the NW portion of Michigan's lower peninsula.

A single uncorrelated sweep of the surface vibrator was easily seen with the naked eye. The sweep (10 seconds long, 18 Hz to 360 Hz) varied greatly in strength on both the hydrophone and geophone data with a peak around 35 Hz. It disappeared into the ambient noise when the sweep approached the 160 Hz region, approximately half way through the 10 second sweep.

Thus we can say that this 6,000 lbs vibrator, employing no "ground force" capability, produces a peak to peak signal of approximately 3 X 10-5 cm/sec on a vertical geophone at a depth of 1,485 ft at the MTU test site. Similarly we find a signal of 1×10^{-7} micoPascals on the hydrophone.

Ambient Noise

The ambient seismic noise observed at 1,485 ft in the boreholes at the Mich. Tech. Test Site is the floor for our amplitude measurements. During our data acquisition we made periodic measurements of the background noise. Our observations varied from a peak to peak value of approximately 1×10^{-6} cm/sec to 1×10^{-5} cm/sec over a frequency band from 200 Hz to 800 Hz.

The literature does not contain data in that frequency band but it does provide data (Frantti, 1963) nearby (100 Hz). We have reproduced Frantti's Michigan noise data here.

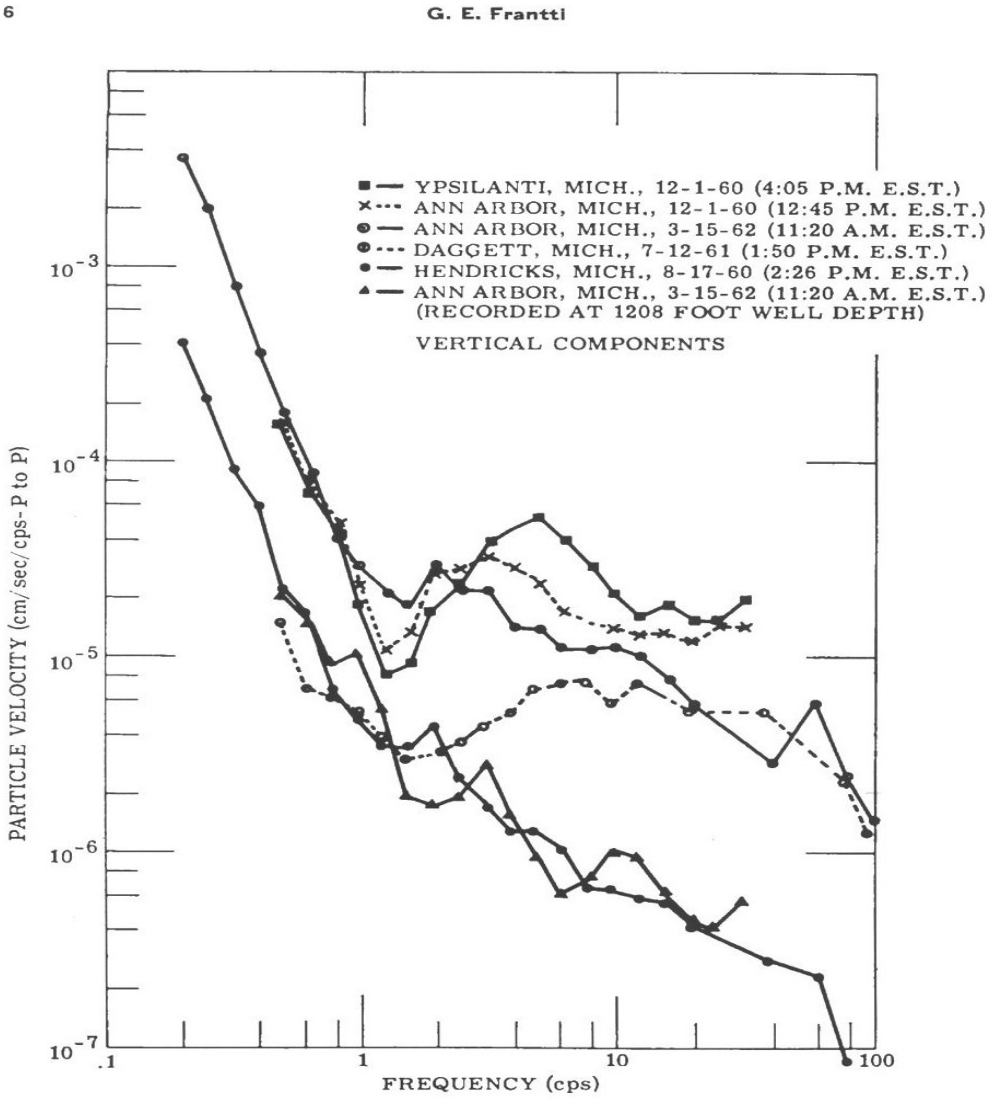

Figure 53 Seismic noise levels from Frantti (1963) for places in Michigan. The borehole measurement from Ann Arbor is lower than our measurement Near Traverse City because special efforts were made in the Ann Arbor borehole to decouple the seismometer package from the surface. The Baker Atlas sonde was connected to the surface with an armored cable.

One can see that our noise floor compares favorably with Frantti's data. Note that Frantti found a wide variation in noise as a function of location in Michigan while we found a smaller variation as a function of time.

Thus the noise levels used in this research at the Michigan Tech Test Site do not constrain the results i.e. signal to noise ratios could not be significantly improved at any other site in Michigan.

Measurement Protocol for the Future

The site is continuously available, for the foreseeable future, for similar tests of tools. Operators can provide their tools and fund the costs of making the measurements. We will attempt to "piggyback" measurements of tools with other operations at the site, or with measurements of other tools, in order to reduce cost. If the measurements are funded entirely by a private company or institution, the results need not be made public; however, we feel that the true benefit of the protocol established, and the availability of the site, will only be realized if the measurements are widely available.

The authors of this report are the main contacts to arrange for use of the site.

Conclusions

Four seismic sources were tested at the Michigan Technological University's Test Site for signal amplitude level and frequency content, three were downhole sources and one was a surface vibrator. The three downhole sources were not seen above ambient seismic noise levels (10^{-6} peak to peak cm/sec to 10^{-5} peak to peak cm/sec) but the surface vibrator was clearly observed. The small surface vibrator (6,000 lbs of force) produced peak to peak signal levels of 4.5×10^{-5} cm/sec at approximately 35-40Hz. Indications of one downhole source (Clean Wells Ltd) was seen in the spectra of both hydrophone and geophone data.

Reference

Frantti, G. E. (1963), The Nature of High-Frequency Earth Noise Spectra, Geophysics, Vol. 28, No. 4.

Capillary-physics mechanism of elastic-wave mobilization of residual oil

Igor A. Beresnev[*], Wayne D. Pennington[‡], and Roger M. Turpening[‡]

[*]Department of Geological and Atmospheric Sciences, Iowa State University, 253 Science I, Ames, Iowa 50011-3212, Tel: 515-294-7529, Fax: 515-294-6049, E-mail: beresnev@iastate.edu.

[‡]Department of Geological and Mining Engineering and Sciences, Michigan Technological University, 1400 Townsend Dr., Houghton, MI 49931, E-mail: wayne@mtu.edu, roger@mtu.edu

[manuscript is in press, GEOPHYSICS]

ABSTRACT

Much attention has been given to the possibility of vibratory mobilization of residual oil, although there has been lack of understanding of an underlying physical mechanism that could explain variable field experiences. Such a mechanism can be found in the physics of capillary entrapment of oil ganglia. The residual oil is entrapped because of the resisting capillary forces that prevent free motion of a non-wetting fluid. A finite external pressure gradient, exceeding the "capillary-barrier" threshold, needs to be applied to carry the ganglia through. The application of vibrations is equivalent to the addition of an oscillatory "inertial" forcing to the constant pressure gradient. When this extra forcing acts along the gradient and the threshold is exceeded, instant "unplugging" occurs and at least one end of the ganglion may move through the constriction, while, when the vibration reverses direction, the flow is still plugged and the ganglion only partially moves back. This asymmetry creates an average non-zero flow over one period of vibration, explaining the mobilization effect. Minimum-amplitude and maximum-frequency thresholds apply for the mobilization to occur. The criteria of a ganglion's mobilization involve the parameters of both the medium (pore geometry, interfacial and wetting properties, and fluid viscosity) and the oscillatory field (amplitude and frequency). The medium parameters vary widely under natural conditions. It follows that an elastic wave with a given amplitude and frequency will always mobilize a certain subpopulation of ganglia leaving others intact; in this sense, the vibratory field will *always* produce a certain mobilization effect. The exact macroscopic effect will nonetheless be hard to predict, as it will represent a cumulative response of the

populations of ganglia with unknown parameter distributions. Variability of reservoir responses to vibratory stimulation should thus be expected.

INTRODUCTION

The problem of incomplete oil recovery has been among the biggest challenges of petroleum industry. It is well known that, even after water flooding, on average two thirds of the oil remains entrapped in the reservoir in form of isolated ganglia (or "blobs") (e.g., Payatakes, 1982). The possibility of vibratory mobilization of the residual oil has received much attention over the last years, mostly due to its potential low cost and environmental friendliness (e. g., Beresnev and Johnson, 1994; Hilpert et al., 2000; Roberts et al., 2001, 2003; Poesio et al., 2002). With field tests proceeding around the world and mixed results being their most consistent feature, the question that has often been asked is why low-frequency vibrations *should* mobilize the residual oil? Is there an underlying mechanism that could explain the variety of field experiences? This predicament reflects the continuing need for a physical framework in which to understand the effect of vibrations on reservoir fluids, which would ideally explain how the changes in the vibration parameters (frequency, amplitude) or reservoir parameters (pore geometry, wetting properties, oil viscosity, etc.) would affect the stimulation result. Since realistic porous media are complex and not amenable to a deterministic treatment, a generic mechanism would have to be sought at an elementary, pore-scale, level, and then applied to a particular fluid or rock type.

Beresnev and Johnson (1994) reviewed the known physical mechanisms that could potentially enhance fluid percolation when a porous medium is irradiated with elastic waves, both in the ultrasonic (high-intensity) and seismic (low-intensity) ranges. Providing such a review is not the purpose of this article. In terms of reservoir stimulation, the ultrasonic treatment is not of considerable practical interest. The ultrasound effect on oil properties may be significant simply due to energy absorption; however, such an affect is limited to at most several meters around the source. The primary application of ultrasonic treatment is therefore in near-wellbore cleaning, which is different from the subject of this paper. We are interested in describing the mechanism that could explain why the *low-frequency* vibrations, producing generally linear deformations of the porous space, could still produce the mobilization effect. We base our discussion on the progress in understanding the hydrodynamic principles of vibratory mobilization made over the last decade or so, since the appearance of Beresnev and Johnson's review. To find answers to the questions posed, we first consider the physics of oil trapping, which is key to understanding why the vibrations could help overcome it.

PHYSICAL MECHANISM OF TRAPPING

Our "stage" is the later phases of water flooding, when the residual oil forms as isolated ganglia surrounded by water. We assume water as the wetting phase (with contact angle close to zero) and oil as the non-wetting phase (contact angle close to 180º), together forming an immiscible flow. We also assume the existence of an external pressure gradient, applied during water flooding, which attempts to drive the residual oil

through the pores. A common representation of pore geometry is a sequence of large open spaces (pore bodies, or simply "pores"), separated by narrow constrictions (or "throats") (Fig. 1), which we adopt here.

The capillary forces are responsible for trapping the oil ganglia in the pores. Let us consider what occurs to an individual ganglion as it travels through the pore body and encounters a constriction. In the open-pore space, the ganglion is free to move under the effect of the pressure gradient, which causes the outer-pressure difference ΔP across the length of the blob (Fig. 1a). Due to the different wetting properties, the water-oil interfaces (menisci) are curved; this curvature creates an excess pressure on either inner side of the blob (the capillary pressure, P_c) (this pressure is responsible, for example, for the capillary rise of water in vertical glass tubes). Assuming, for simplicity, that the interfaces are spherical, the capillary pressure obeys the Laplace equation,

$$P_c = 2\sigma/R, \tag{1}$$

where σ is the oil/water interfacial tension and R is the menisci radius. For simplicity, we neglect the effect of ganglion velocity on the contact angle. The internal capillary pressure is then balanced inside the blob and produces no net effect on the ganglion motion.

We next consider the situation when the blob hits the constriction (Fig. 1b). When passing into the constriction, the meniscus radius on the right (R_R) becomes smaller than the radius on the left (which is still R), which, according to equation (1), increases the internal capillary pressure on the right side to P_c^+. The internal pressure

imbalance $P_c^+ - P_c$ is created that acts against the external gradient. It appears as if the blob "resisted" passing through the constriction. If the constriction becomes sufficiently narrow, the ganglion stops altogether; at this point, the criterion

$$\Delta P = P_c^+ - P_c = 2\sigma(1/R_R - 1/R) \tag{2}$$

is satisfied. The ganglion is trapped.

A similar phenomenon is known in physiology; when an air bubble is introduced into a blood vessel, it can block the blood flow if it encounters a constriction. This is why introduction of bubbles into blood circulation is considered dangerous.

Note that the effect of entrapment is exclusively due to capillary phenomena. For example, if the surface tension of oil/water interface were close to zero, or in a hypothetical case of pipe-like straight pore channels, the oil would have never been trapped and would have flowed inhibited by the normal Newtonian viscosity only. Nearly all oil would have eventually been recovered under any non-zero pressure gradient (assuming total pore connectivity).

For the entrapped oil, as in Figure 1b, the external pressure gradient needs to exceed a certain "unplugging" threshold to overcome the capillary barrier and push the blob through the constriction. This threshold value is controlled by the geometry of the constriction, properties of oil/water interface, and properties of the solid (through the contact angle); it will thus be highly variable for the conditions encountered in natural porous media. If we sketch a plot of the flow rate as a function of constant pressure gradient, we will obtain a schematic diagram in Figure 2 (solid line). The flow begins

when the unplugging threshold (∇P_0) is exceeded. The dashed line shows what would be expected for a "normal" Darcy flow, in which the flow rate is proportional to the pressure gradient. Clearly, due to capillary trapping, the flow of oil ganglia through the constricted pores deviates from the Darcy law. The form of the diagram shown as a solid line is a variant of the Bingham behavior, a special case of non-Newtonian rheology (Middleton and Wilcock, 1994, p. 339). It is also often called the yield-stress rheology. The physical meaning of the Bingham behavior is that, at low forcing level, the fluid is immobile, and the flow commences only after the yield stress is applied. We conclude that the residual-oil flow is governed by the Bingham rheology.

Some waxy crude oils exhibit the yield-stress behavior even as a single phase. Their response to the external pressure gradient will be identical to the solid line in Figure 2, although no capillary phenomena are involved. The mechanisms of elastic-wave mobilization of residual oil in water-flooded reservoirs and of a single viscoelastic fluid filling the entire pore will thus be totally equivalent (Iassonov and Beresnev, 2003).

This problem formulation thus restricts our attention to the flow of disperse isolated non-wetting ganglia in a wetting environment, corresponding to a typical scenario of secondary oil recovery from a water-flooded reservoir. If the oil were a wetting phase, the capillary entrapment in the sense considered would not exist. The entrapment scenarios plausible under limited circumstances for wetting oil are beyond the scope of this paper. Also, although seismic-frequency vibrations in some instances may cause the enhancement in the flow of continuous one-phase fluid (Chrysikopoulos and Vogler, 2004) or dissolution/breakup of isolated ganglia in an immiscible two-phase flow

(Vogler and Chrysikopoulos, 2002), this article does not investigate mechanisms of such phenomena.

MECHANISM OF VIBRATORY MOBILIZATION OF ENTRAPPED GANGLIA

Amplitude effect

It is now possible to address the issue of how application of low-frequency vibrations could mobilize the ganglion entrapped in the pore throat as illustrated in Figure 1b. Let us turn to a modification of the diagram in Figure 2 as shown in Figure 3. Let us assume that the system is under an external static pressure gradient ∇P_s, whose value is below the threshold ∇P_0 needed to mobilize the flow, and the system resides in static equilibrium. We now consider what happens to the system when vibratory field is applied.

The frequency of vibrations is low and the wavelength is much longer than the length of any isolated ganglion. The solid and the fluid are coupled through a viscous boundary layer only. When the pore wall moves under the effect of a longitudinal wave, only this thin boundary layer moves in phase with the wall; the motion of the fluid away from the wall will in general lag behind (without the loss of generality, we consider only the motion parallel to the pore axis). The effect of the wave is therefore to create a relative motion of the solid and the fluid phases; for the dynamics of the fluid, this is equivalent to the addition of an external oscillatory forcing (with amplitude F_{osc}) acting parallel to the pressure gradient (which is sometimes called "inertial forcing"). This is

schematically illustrated in Figure 3 as the vibratory forcing around the equilibrium point.

Due to the long wavelength, the added oscillatory motion is the same across the length of the blob. The exact amplitude of the body force added to the fluid due to vibrations for cylindrical channel geometry is $F_{osc} = \rho_f a_0$, where ρ_f is the density of the fluid and a_0 is the amplitude of the acceleration of the wall (e. g., Biot, 1956, equation 2.4). The dynamic flow in the channel will be a response of the fluid to this inertial forcing. Clearly, the response will depend on fluid viscosity, the lower the viscosity the stronger the effect; it may also depend on wetting properties. In the following, we will use the term "amplitude" of vibrations in the sense of the acceleration amplitude a_0 that controls the body forcing.

Let us now consider the effect of the added periodic forcing on the fluid motion. We will center our discussion on the case when $\nabla P_s > \nabla P_0/2$ (as in Figure 3); the need for this assumption will soon become clear. Hereafter, the positive direction of forcing (and the flow) is along the external gradient (from high to low pressure). As Figure 3 illustrates, the condition for the mobilization is that the total peak forcing (the sum of the constant and oscillatory parts) exceed the unplugging threshold, $F_{osc} + \nabla P_s > \nabla P_0$. When the vibrational amplitude F_{osc} is sufficiently small, there will be no vibrational effect on the flow (the total forcing will be entirely within the "no-flow" zone, where the forces pushing the ganglion to the right are exactly counterbalanced by the resisting capillary force). However, when the vibratory amplitude exceeds $\nabla P_0 - \nabla P_s$, the total forcing starts to spend part of its cycle in the "flow" zone and the rest of the cycle in the "no-flow" zone. While in the "flow" zone, the ganglion is unplugged and receives a "push" from the total forcing, before reversing direction and moving back into its equilibrium

position, where it is held against the constriction. If an individual "push" is sufficient to move the (right) meniscus through the constriction, then the non-zero average flow over one cycle can resume.

Since the beginning of the "flow" zone is immediately past the narrowest point in the throat, once the downstream meniscus has moved beyond that point, the resisting capillary force starts to progressively decrease (the radii of the right and left menisci become closer and closer), creating a progressive increase in the net forcing. As a result, the ganglion *accelerates* upon exiting, emphasizing the asymmetry between the "no-flow" and "flow" zones.

This process is illustrated in Figure 4, which shows (for the oscillatory amplitude still small enough, $F_{\text{osc}} < \nabla P_s$) the formation of the non-zero average total forcing above ∇P_0 (solid line) for the ganglion's movement just past the narrowest cross-section, such that the ganglion experiences the translational displacement to the right. We could conveniently call this a "rectification" effect. Clearly, the rectification is due to the directional asymmetry in the system response to oscillatory forcing around the equilibrium point: while forcing "to the right" may create an accelerated flow during the "unplugged" time, forcing to the left may not. The external vibrations simply exploit this asymmetry. Note that the vibrations cannot create a non-zero net flow on their own without the presence of an external gradient counterbalanced by the capillary force, as they will simply oscillate the fluids back and forth with zero average.

After a certain number of vibrational periods, the ganglion is moved forward a sufficient distance to be entirely released from the constriction and be able to flow freely. This final stage of the ganglion motion is illustrated in Figure 1c.

A similar phenomenon of the formation of rectified motion under periodic excitation is known in mechanical engineering as "vibrational transport". Suppose we have a mass resting on a surface whose coefficient of static friction is directionally asymmetric, i. e., smaller for forcing in one direction and greater in the other. An example would be fish lying on a conveyor belt (Kalinitchenko and Sekerj-Zenkovitch, 1998, p. 249; Blekhman, 2000, chap. 9). Since static friction is different in the two opposite directions of periodic forcing, the displacement of the mass on the belt will be larger in one half-period than in the other, resulting in a non-zero net displacement. The physical mechanisms of the "rectification" in the above two cases are analogous, being an asymmetric response of the system to the forcing in opposite directions.

For a fixed frequency, after the average ganglion flow has been initiated, the flow rate will initially grow with amplitude. However, when the amplitude reaches the point when it equals the external pressure gradient, $F_{\text{osc}} = \nabla P_s$, it will start creating a non-zero total forcing in the direction opposite to the gradient (when the vibration reverses direction) as well. When the amplitude grows sufficiently large, the ganglion will start spending most of its time in the "flow" zones in Figure 3, both in the positive and the negative half-periods, since neither the capillary forces nor the external gradient will restrict its motions, respectively, and the amplitude effect will eventually saturate. At large amplitudes, the flow therefore will return to the Darcy regime and will represent a unidirectional motion driven by the gradient ∇P_s with a superimposed oscillatory component. The saturation amplitude will of course depend on the value of the constant gradient (location of the static point ∇P_s in Figure 3). One can predict, therefore, that, for

practical purposes of flow enhancement, an indefinite increase in the amplitude of vibratory excitation will not result in the proportional increase in the enhancement effect.

These features of the flow obtained from simple physical reasoning can be illustrated by the results of calculations using exact equations of fluid dynamics (Graham and Higdon, 2000) or simple model equations (Iassonov and Beresnev, 2003). For example, Figure 5 shows the flow rate of a spherical droplet (averaged over the cycles needed to mobilize it) through the constriction as a function of the amplitude of oscillatory forcing, demonstrating the saturation effect (modified from Graham and Higdon, 2000, their figure 15). The flow rate is normalized by the rate of a single-phase fluid with the same viscosity (viscosities of oil and water are assumed equal) under the same pressure gradient, while the amplitude F_{osc} is normalized by the pressure gradient ∇P_s, which is chosen to be slightly above half ∇P_0. Other details of numerical calculations can be found in the figure caption. When the amplitude of vibrations $F_{osc}/\nabla P_s$ exceeds approximately 1, "unplugging" occurs. Because the peak total forcing, divided by ∇P_0 is in this case $(\nabla P_s + F_{osc})/\nabla P_0 = (\nabla P_s/\nabla P_0)(1 + F_{osc}/\nabla P_s) \approx 0.5\,(1 + F_{osc}/\nabla P_s) \approx 1$, "unplugging" corresponds to the total forcing equal to the unplugging threshold ∇P_0, as we expected. Also, as expected, further increase in the amplitude initially enhances the flow until saturation is quickly reached at $F_{osc}/\nabla P_s \approx 4$. A peak in the curve occurring before it levels off can be understood considering that the ganglion flow rate is normalized by the single-phase rate under the pressure gradient ∇P_s acting alone. At F_{osc} at which the peak occurs, the ganglion spends part of the cycle in such a position beyond the narrowest point in the constriction where the capillary force starts to act along (not opposite to) the gradient (the meniscus radius on the right becomes greater

than one on the left); as a result, all contributing forces (the gradient, the oscillatory force, and the capillary force) add up in the same direction. The resulting average forcing over the cycle exceeds ∇P_s, which explains the peak. As the amplitude increases still further and the menisci spend most of their time out of the constriction, the average flow returns to the Darcy regime under the gradient ∇P_s, and the peak disappears.

The return of the flow to the Darcy regime when a sufficient oscillatory forcing amplitude is exceeded is illustrated in Figure 6 (Iassonov and Beresnev, 2003, their figure 8). This set of curves presents the ganglion's period-average flow rate as a function of the external pressure gradient, with the amplitude of oscillatory forcing as a parameter. The flow rate is normalized by the rate of the single-phase oil under the gradient equal to the unplugging threshold ∇P_0, and both the pressure gradient (∇P_s) and the oscillatory-forcing amplitude (F_{osc}) are non-dimensionalized by ∇P_0. The bottom curve represents the Bingham flow (the amplitude $F_{\text{osc}}/\nabla P_0 = 0.5$ is below the amplitude threshold needed to mobilize the flow) (Iassonov and Beresnev simulated a slightly different variant of Bingham flow compared to Fig. 2). When the vibratory amplitude increases ($F_{\text{osc}}/\nabla P_0 =$ 1.0.), "unplugging" occurs at a lower gradient $\nabla P_s/\nabla P_0 \approx 0.5$ (second curve from bottom). The peak total forcing, divided by ∇P_0, then equals $(\nabla P_s + F_{\text{osc}})/\nabla P_0 = 0.5 +$ 1.0 = 1.5, which is consistent with our expectations and the unplugging level found numerically by Graham and Higdon (2000) (see Fig. 5). When the vibratory forcing reaches the value of four unplugging thresholds ($F_{\text{osc}}/\nabla P_0 = 4.0$, top curve), the flow becomes virtually unrestricted and obeys the Darcy law. Figure 6 demonstrates that the effect of vibrations is to effectively lower the value of the constant pressure gradient

needed to mobilize the flow. When the vibration amplitude is sufficiently large, nearly any finite pressure gradient is sufficient to move the ganglion.

We began this section with the assumption that $\nabla P_s > \nabla P_0/2$. As seen in Figure 3, when $\nabla P_s < \nabla P_0/2$, an interesting phenomenon may occur such that, when the amplitude of vibrations just exceeds ∇P_s, a period-average flow may be generated in the direction opposite to the gradient (exploiting the same kind of directional asymmetry as considered above). This average flow is short-lived, though. It can only be generated while the ganglion is firmly pressed against the constriction during part of the cycle; once it drifts slightly to the left, losing contact with the constriction, the average net force turns to zero (as the ganglion starts simply oscillating back and forth), and the ganglion is pushed back to the constriction by the pressure gradient. The case of $\nabla P_s < \nabla P_0/2$ does not therefore represent any practical interest.

Frequency effect

Since the ganglion accelerates upon exiting the throat, its resulting net displacement over one period (and hence the average flow rate) becomes a nonlinear function of time; as a result, this displacement will depend on the amount of time spent in the "unplugged" position, which is controlled by the oscillation frequency. For a given amplitude, therefore, the mobilization effect will also exhibit the frequency dependence. At low frequencies, this time is longer, and the droplet receives a stronger "push" than at higher frequencies of the same forcing amplitude. It follows that the effect will inversely depend on the frequency, which could first seem somewhat counterintuitive but can be

understood considering that the acceleration amplitude is kept constant. Above a certain "threshold" frequency, the effect may disappear altogether. We thus infer that, in addition to the existence of a minimum-amplitude threshold for the mobilization, there also is a maximum-frequency threshold.

The lack of "push" at a higher frequency can be compensated for by the increase in the amplitude. We can expect therefore that the threshold amplitude of vibratory forcing needed to initiate the flow will increase with the frequency. The frequency and the amplitude dependence of the period-average flow rate can be summarized in a family of curves schematically exhibited in Figure 7, which has the frequency as a parameter. The curves are plotted for the range of amplitudes below saturation and demonstrate the existence of both the minimum amplitude and maximum frequency for the mobilization to occur. As the frequency increases (from curve 1 to 3), the corresponding threshold amplitude F_{th} also increases. For a given amplitude, the effect increases with decreasing frequency. At some forcing levels (say, F_{th2}), there is a frequency (curve 3) at which the flow is still blocked, while it is mobilized at a lower frequency (curve 1). These qualitatively predicted features are indeed obtained theoretically (Averbakh et al., 2000, their figure 5) and experimentally (Zaslavskiĭ, 2002, author's figure 1) (the authors consider a different capillary system with same physics of trapping).

The value of the threshold frequency for a given amplitude can be estimated from a simple observation that, for the mobilization to occur, the distance traveled by the ganglion in the "unplugged" position during one period of vibrations should represent a finite fraction of the throat length (it cannot be infinitesimally small). If the ganglion velocity in the unplugged position is U, the throat length is L, and the period of vibrations

is T, then the ratio $L/(UT)$ should take a finite value; from this condition, the minimum period T_{min} can be calculated. The numerical fluid-dynamics calculations provide the value of the threshold frequency, $f_{max} = 1/T_{min}$, of $f_{max} \approx (2 \div 5)U/L$, above which the flow for a given amplitude is stopped (Graham and Higdon, 2000, their figure 22). The "unplugged" flow rate U in this equation can be estimated from the Darcy (or Poiseuille) law, and f_{max} will therefore exhibit an inverse dependence on viscosity, as it certainly should, as a more viscous fluid travels a smaller distance over the given "unplugged" time. Because the Darcy (Poiseuille) velocity U is also proportional to the forcing level, f_{max} will increase linearly with the amplitude, as also was demonstrated by Graham and Higdon (2000, section 7.5). This trend will continue until the frequency becomes high enough that the fluid stops responding to vibrations, that is, when the fluid's characteristic response time to dynamic excitation, $\tau = \rho_f r^2/\mu$ (Johnson, 1998, p. 9-11), where r is the radius of the channel and μ is the dynamic viscosity, becomes small compared to T. The specific coefficient in the equation for f_{max}, though, should be used with caution, as it was obtained for a capillary tube with sinusoidal profile (periodic constrictions) and a single combination of problem parameters (Graham and Higdon, 2000). This simple reasoning also assumes laminar flow, at rates where turbulent effects still do not occur, and certainly cannot be extrapolated to other regimes.

IMPLICATIONS FOR VIBRATORY STIMULATION

Prediction of the stimulation effect

We should consider the implications of the above physics of trapping and vibratory mobilization of the residual oil for the practical seismic-wave stimulation of water-flooded reservoirs. We should also relate the corollaries of the physical mechanism to the experiences encountered in the field tests.

Summarizing, we first conclude that the vibration of any given amplitude and frequency will *always* produce a mobilization effect on the residual oil. Each in the population of ganglia trapped in the reservoir resides in an equilibrium with the external pressure gradient and is characterized by its individual "gap" ∇P_0 - ∇P_s keeping it away from the mobilization (Fig. 2). This capillarity-controlled gap in a natural medium will be highly variable, depending on a particular porous geometry and interfacial and wetting properties at contacts of all three phases. These factors, plus the history of water flooding, will also control the amount of entrapped oil. In addition, the effect of the oscillatory forcing will depend on fluid viscosity, and viscosity will also control the maximum frequency that can produce the mobilization effect. It follows that there will always be a certain sub-population of ganglia for which the given amplitude and frequency will satisfy the mobilization criteria and which will therefore be mobilized, while other ganglia will remain intact. In this sense, a certain stimulation effect can always be expected, and it will grow with increasing amplitude (until saturation) and decreasing frequency. For these reasons, the magnitude of the stimulation effect for a particular reservoir is hardly predictable, as it will represent a statistical average over unknown distributions of ganglia and pore and fluid parameters. Every reservoir may be expected to show its individual response to seismic stimulation, from a sizeable flow enhancement to insensitivity. This type of behavior coincides with the character of (still

scanty) printed and oral reports of field testing of vibroseismic stimulation in various environments, available to the authors (e. g., Beresnev and Johnson, 1994); it is important to note, though, that such results should be expected from the underlying mechanism.

A reasonable field strategy would be to approach a particular stimulation prospect with a variety of amplitudes and frequencies (if technically and economically feasible) and document the results to select the most efficient mode (as has often been done, see Beresnev and Johnson, 1994). The economic side of the stimulations should also be borne in mind, such as the cost/benefit ratio, including the cost of sonic-energy delivery (from surface or borehole) and the benefit of additional recovered oil. The costs and potential benefits will determine the advisability of stimulations.

Criteria for successful stimulation

The above mechanism description also allows us to approach, at least in a general sense, the criteria for successful stimulation. Beresnev and Johnson (1994, p. 1013) summarized, based on published field evidence, the empirical criteria for successful vibroseismic treatment of oil reservoirs; we note that the roots of all of them can now be traced to the underlying capillary mechanism (as indicated in the parentheses below):

1) The shallower the reservoir the stronger the effect (the mobilization effect increases with amplitude);
2) Water percentage no lower than 90 percent (the residual ganglia are created in advanced stages of water flooding. The number of 90 percent is of course

purely conventional, as the mechanism applies to all water-cut levels as long as isolated non-wetting ganglia remain in the system);

3) The smaller oil viscosity the better (the effect of the vibratory forcing increases with decreasing viscosity);
4) Optimal (resonant) frequencies to be selected (frequencies above a certain threshold may be inefficient).

From our discussion of the physical mechanism of oil trapping, it is evident that the residual oil can also be mobilized by simply increasing the pressure gradient above the unplugging threshold. A question arises as to why to use the vibratory stimulation if the same effect can be achieved by simply raising the injection pressure. The answer is that, in many cases, boosting water flooding may not be a practical solution. For example, one could easily imagine the situation when augmenting the injection pressure would economically or technically be unfeasible, while applying vibrations would be a viable task. A realistic scenario would also be when the increased water injection only forces more water to flow along preferential paths of least resistance (such as fractures), without penetrating into untapped pools of oil (the bypassing effects). In such cases, the delivery of high pressures into hydrodynamically "insulated" volumes would be problematic; however, this problem would not affect the delivery of seismic energy, which, with little discrimination, is carried to every point of the porous space.

TASKS FOR THEORETICAL AND EXPERIMENTAL WORK

The mechanism of vibrations working against the capillary barrier explains the possibility of vibratory mobilization of residual oil. It also indicates that the effect exhibits both the amplitude and frequency thresholds and also depends on a number of other parameters, including fluid and rock properties, individual pore geometry, and the value of static pressure gradient in every pore. A full, practically useful theoretical description of the mobilization effect would be achieved if closed-form analytical solutions were found from the exact hydrodynamics of the two-phase immiscible flow with capillarity, which would relate in a physically insightful way all the parameters to the average flow rate. An ultimate theoretical goal for the vibratory stimulation would be to predict the amplitude of seismic waves that would produce a given increase in the oil flow rate. This task has not been completed yet due to the absence of such theoretical solutions.

An implementation of this task (if at all feasible) would possibly combine the advantages of the approaches represented, for example, by Graham and Higdon (2000) on one side and Iassonov and Beresnev (2003) and Hilpert et al. (2000) on the other. Graham and Higdon (2000) solve a complete hydrodynamic problem, which, due to its complexity, only allows numerical treatment. The resulting quantitative results (such as those presented in Fig. 5), although being a milestone in illuminating the physics of vibratory mobilization, would be hard to use for practical calculations (e. g., predicting the seismic amplitude needed for mobilization), as they do not provide the means of exploring the full parameter space (have been obtained for fixed values of all other parameters). Due to a large number of the parameters involved, their wide variability in

natural systems, and the possibility of their complex interactions, having such means is important.

Iassonov and Beresnev (2003) use simpler model equations and a number of simplifying assumptions, which allowed them to obtain analytical solutions for the flow rate under the effect of vibrations. However, this work has a disadvantage of not considering the capillary geometry of the constricted flow that provides an explicit trapping mechanism. The authors had to postulate an implicit trapping mechanism; as a result, the estimates of seismic-wave intensities needed to mobilize the flow could be unreliable. This can probably be corrected in a straightforward manner in future work. Hilpert et al. (2000) consider the exact capillary geometry of the constricted flow but do not calculate the effect of the vibrations on the flow rate. Future theoretical work will probably see a combination of the strong aspects of all these approaches, providing more powerful predictive tools.

Another aspect of a realistic porous medium is that, even if one could calculate the amplitudes of seismic waves sufficient to achieve a tangible flow rate of residual ganglia under the given pressure gradient and a set of medium and wave parameters, the realistic porous space is still stochastic in nature. Understanding how pores and throats of a given geometry will respond to a wave excitation is only half-a-solution; the rest would be to predict how the flow induced in a number of different pores, connected in two- or three-dimensional patterns, will combine into a spatially average flow. This is the realm of pore-network models, whose development should be part of building the theory of vibratory stimulation, although the discussion of pore networks is beyond the subject of this article.

Another important methodological problem is to know whether the seismic energies, required to produce a significant effect on the residual oil, could realistically be delivered to the reservoir volumes from the available sources or tools. To deliver high sonic intensities, the sources should probably operate from deep boreholes. The issue is then to find out what seismic amplitudes can be created by the existing downhole sources in the reservoir environments. This is the task for experimental measurements related to the possibility of elastic-wave mobilization of oil.

Laboratory work on the direct verification of mobilization phenomena in controlled environments (e. g., Roberts et al., 2001; Poesio et al., 2002) should be continued. This creates a test ground for the existing theories of flow enhancement by vibrations, including this one. Clearly, the predictions of the mechanism outlined in this paper are directly verifiable in the laboratory and should be experimentally addressed.

The directions of future work are thus well defined and could resolve some long-standing quantitative issues of vibroseismic stimulation of residual-oil recovery.

ACKNOWLEDGMENTS

This work was supported by the Department of Energy award DE-FC26-01BC15165 and the National Science Foundation award EAR-0125214. We are grateful to P. Iassonov and two anonymous referees for reviewing the manuscript.

REFERENCES

Averbakh, V. S., S. N. Vlasov, and Yu. M. Zaslavsky, 2000, Motion of a liquid droplet in a capillary under the action of static force and an acoustic field: Radiophysics and Quantum Electronics, **43**, 142-147.

Beresnev, I. A., and P. A. Johnson, 1994, Elastic-stimulation of oil production: A review of methods and results: Geophysics, **59**, 1000-1017.

Biot, M. A., 1956, Theory of propagation of elastic waves in a fluid-saturated porous solid. II. Higher frequency range: Journal of the Acoustical Society of America, **28**, 179-191.

Blekhman, I. I., 2000, Vibrational mechanics: World Scientific.

Chrysikopoulos, C. V., and E. T. Vogler, 2004, Acoustically enhanced multicomponent NAPL ganglia dissolution in water saturated packed columns: Environmental Science and Technology, **38**, 2940-2945.

Graham, D. R., and J. J. L. Higdon, 2000, Oscillatory flow of droplets in capillary tubes. Part 2. Constricted tubes: Journal of Fluid Mechanics, **425**, 55-77.

Hilpert, M., G. H. Jirka, and E. J. Plate, 2000, Capillarity-induced resonance of oil blobs in capillary tubes and porous media: Geophysics, **65**, 874-883.

Iassonov, P. P., and I. A. Beresnev, 2003, A model for enhanced fluid percolation in porous media by application of low-frequency elastic waves: Journal of Geophysical Research, **108**, ESE 2-1 – 2-9.

Johnson, R. W., 1998, The handbook of fluid dynamics: CRC Press.

Kalinitchenko, V. A., and S. Ya. Sekerj-Zenkovitch, 1998, On the immiscible fluid displacement in capillary under oscillating pressure drop: Experimental Thermal and Fluid Science, **18**, 244-250.

Middleton, G. V., and P. R. Wilcock, 1994, Mechanics in the Earth and environmental sciences: Cambridge University Press.

Payatakes, A. C., 1982, Dynamics of oil ganglia during immiscible displacement in water-wet porous media: Annual Review of Fluid Mechanics, **14**, 365-393.

Poesio, P, G. Ooms, S. Barake, and F. van der Bas, 2002, An investigation of the influence of acoustic waves on the liquid flow through a porous material: Journal of the Acoustical Society of America, **111**, 2019-2025.

Roberts, P. M., I. B. Esipov, and E. L. Majer, 2003, Elastic wave stimulation of oil reservoirs: promising EOR technology? The Leading Edge, **22**, 448-453.

Roberts, P. M., A. Sharma, V. Uddameri, M. Monagle, D. E. Dale, and L. K. Steck, 2001, Enhanced DNAPL transport in a sand core during dynamic stress stimulation: Environmental Engineering Science, **18**, 67-79.

Vogler, E. T., and E. V. Chrysikopoulos, 2002, Experimental investigation of acoustically enhanced solute transport in porous media: Geophysical Research Letters, **29**, 5-1 – 5-4.

Zaslavskiĭ, Yu. M., 2002, Experimental study of the motion of liquid droplets in a capillary under vibration: Acoustical Physics, **48**, 50-53.

FIGURE CAPTIONS

FIG. 1. Geometry of the immiscible two-phase flow through a porous channel with a constriction, under the effect of external pressure gradient. (a) Blob in the open channel. (b) Right side of the blob in the constriction; the blob is trapped. (c) Blob released by vibrations and driven freely again.

FIG. 2. Average flow rate versus external pressure gradient for the conventional Darcy flow (dashed line) and Bingham yield-stress flow (solid line). An oil ganglion in a constricted pore under the action of external gradient obeys the Bingham law.

FIG. 3. The mechanism of the formation of "rectified" fluid motion under the combined effect of external pressure gradient and oscillatory forcing.

FIG. 4. Temporal changes in total forcing (bold line) creating unidirectional flow.

FIG. 5. Average flow rate (normalized by the flow rate of a single-phase fluid under the same pressure gradient) versus amplitude of vibratory forcing (normalized by the pressure gradient). The ganglion radius is twice the smallest radius of the sinusoidal constriction, the viscosities and densities of oil and water are equal, and the excitation frequency is much smaller than f_{max} (see text) (modified from Graham and Higdon, 2000, their figure 15).

FIG. 6. Average flow rate (normalized by the flow rate of a single-phase oil under the pressure gradient ∇P_0) versus pressure gradient (normalized by ∇P_0). The amplitude of oscillatory forcing is the parameter of the curves (after Iassonov and Beresnev, 2003, their figure 8).

FIG. 7. Average flow rate as a function of amplitude of vibratory forcing, showing the existence of both minimum-amplitude and maximum-frequency thresholds. Frequency is the parameter of the curves.

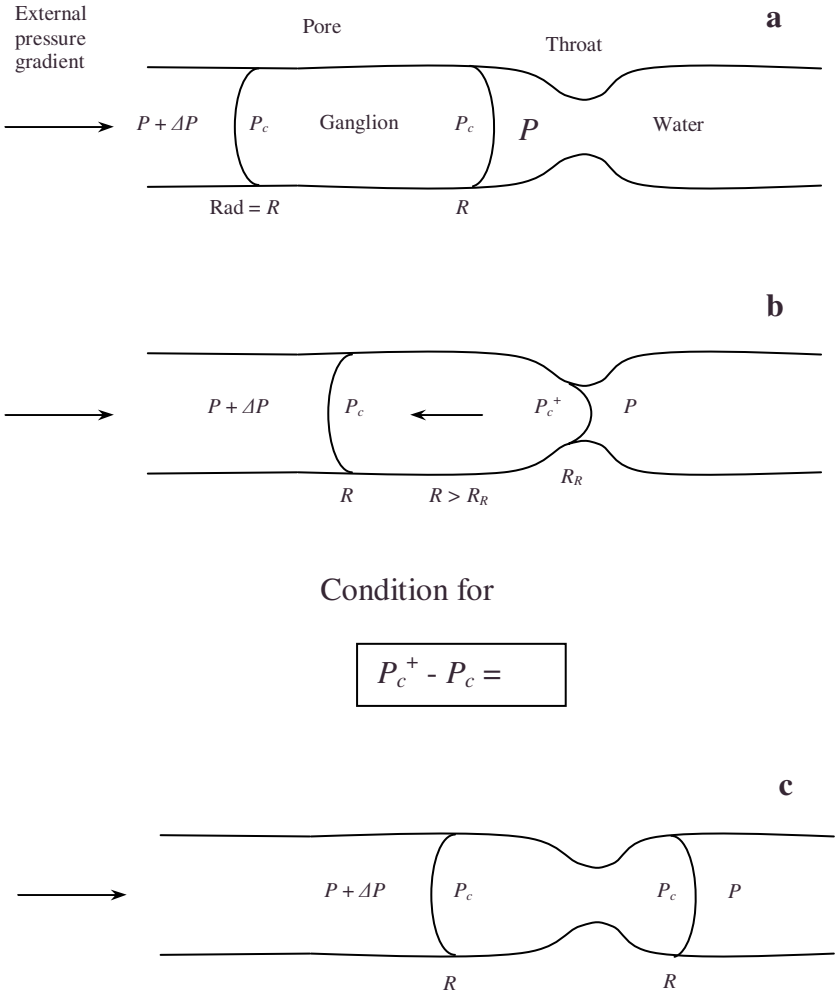

FIG. 1. Geometry of the immiscible two-phase flow through a porous channel with a constriction, under the effect of external pressure gradient. (a) Blob in the open channel. (b) Right side of the blob in the constriction; the blob is trapped. (c) Blob released by vibrations and driven freely again.

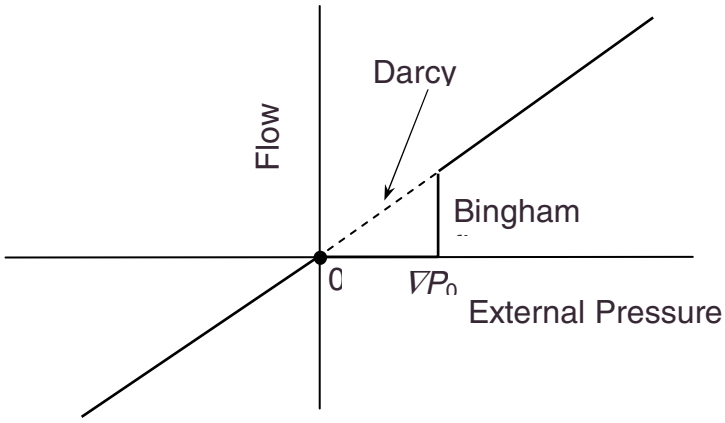

FIG. 2. Average flow rate versus external pressure gradient for the conventional Darcy flow (dashed line) and Bingham yield-stress flow (solid line). An oil ganglion in a constricted pore under the action of external gradient obeys the Bingham law.

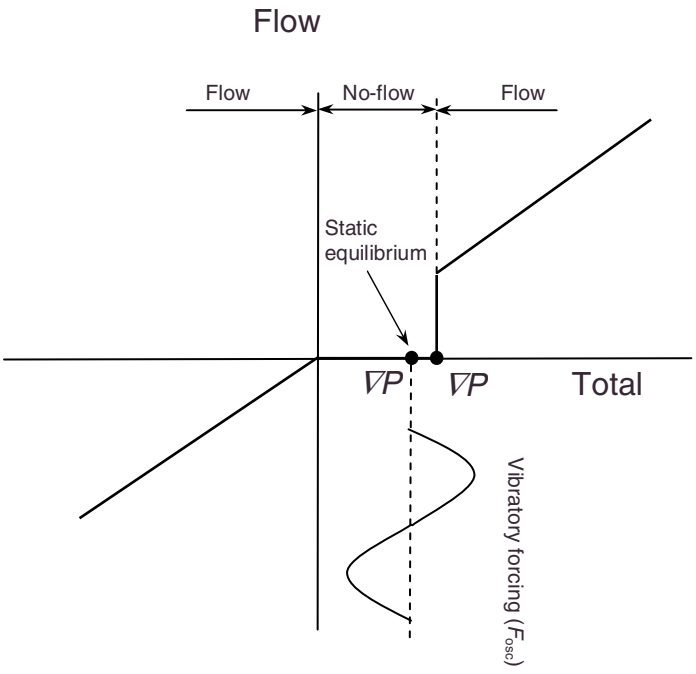

FIG. 3. The mechanism of the formation of "rectified" fluid motion under the combined effect of external pressure gradient and oscillatory forcing.

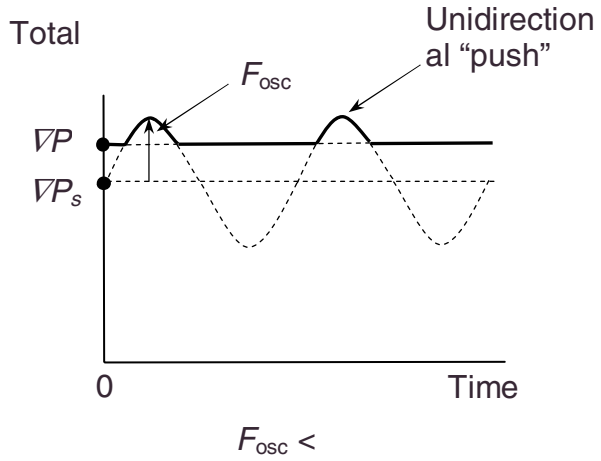

FIG. 4. Temporal changes in total forcing (bold line) creating unidirectional flow.

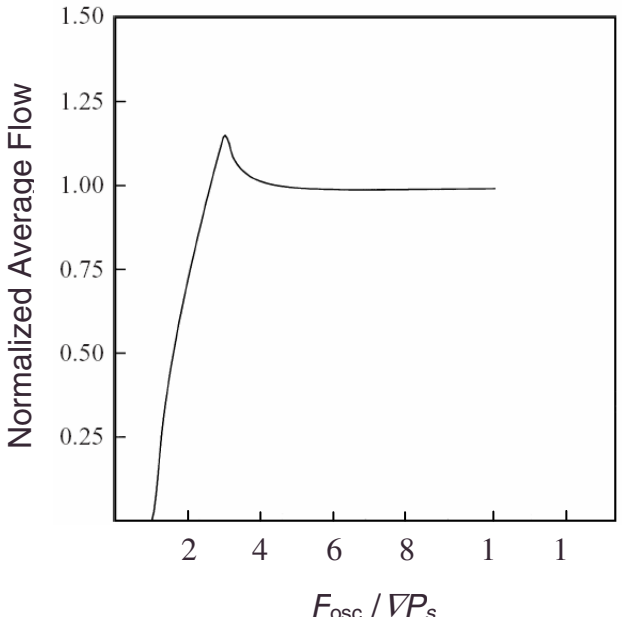

FIG. 5. Average flow rate (normalized by the flow rate of a single-phase fluid under the same pressure gradient) versus amplitude of vibratory forcing (normalized by the pressure gradient). The ganglion radius is twice the smallest radius of the sinusoidal constriction, the viscosities and densities of oil and water are equal, and the excitation frequency is much smaller than f_{max} (see text) (modified from Graham and Higdon, 2000, their figure 15).

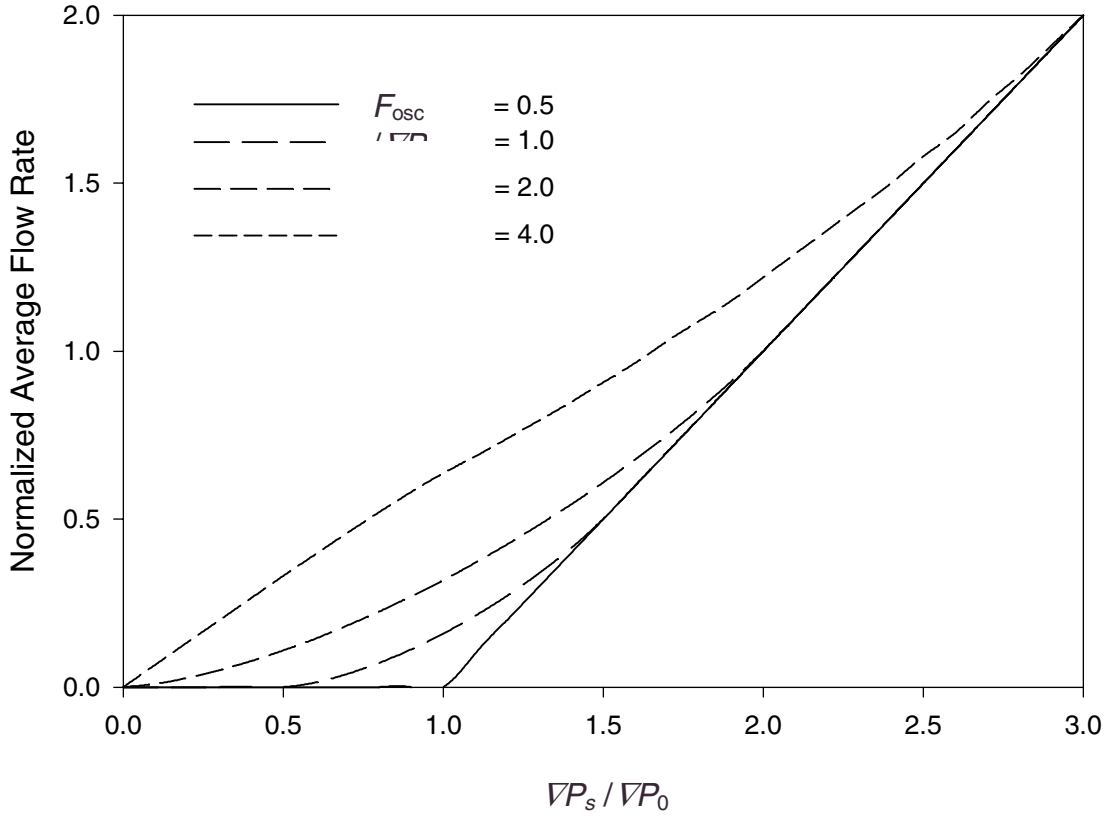

FIG. 6. Average flow rate (normalized by the flow rate of a single-phase oil under the pressure gradient ∇P_0) versus pressure gradient (normalized by ∇P_0). The amplitude of oscillatory forcing is the parameter of the curves (after Iassonov and Beresnev, 2003, their figure 8).

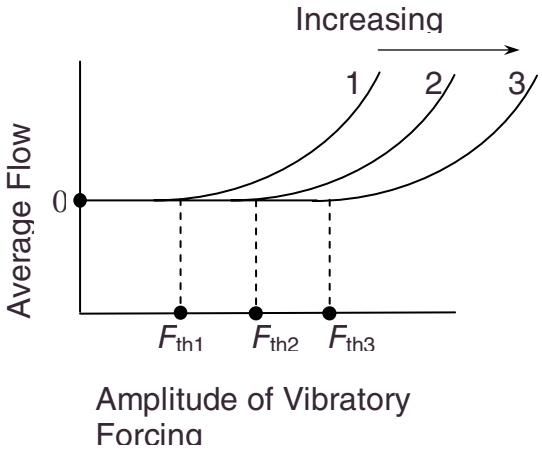

FIG. 7. Average flow rate as a function of amplitude of vibratory forcing, showing the existence of both minimum-amplitude and maximum-frequency thresholds. Frequency is the parameter of the curves.

Appendix B:
Guidelines for Studies of Enhanced Petroleum Production by Sonic Stimulation

The reference list of sonic stimulation studies is strongly anecdotal. Originally, this was due to the nature of the studies, where the improved production was observed after some coincidental event that may or may not have been responsible. Current studies should be scientific, and not anecdotal, if the sonic stimulation was applied with the intent of improving production. This short note is intended to provide guidelines for the scientific analysis and presentation of sonic stimulation studies.

Proper accounting of production history:
The production of all of the wells that could possibly be affected by the stimulation should be reported for a significant time period prior to, during, and, if appropriate, after the stimulation. If the sonic tool was placed in a well, the production history of that well should also be provided. The total production of all of the wells should be included, so that the reader can determine if the reported increased production was a result of, say, shutting in the stimulation well, rather than the act of stimulation itself.

Approximating a "control" case for comparison:
If the experiment involves shutting a well during stimulation, then a comparison should be made with a separate experiment, during which the well is shut in for a comparable period of time, but without stimulation, to allow evaluation of the usual shut-in "flush" recovery that might be expected.

Accounting for other production affects:
All production changes, such as valve replacements, shut-ins, workovers, and so forth, for all of the wells in the area of the study should be reported.

Making the test as scientific as possible:
The goal of all sonic stimulation tests should be to evaluate the quality of improved recovery provided by the exercise. This involves isolating all possible components of the mechanism and testing them separately, to the extent that this is practical. The real world of petroleum production can prevent a purely scientific study in many cases, but there should be an honest attempt to closely approximate such a study.

> Can there be a "control" well?
> In most scientific studies, there is a "control" or similar set of conditions, but with the subject of the study (in this case, the sonic stimulation) missing. This is difficult to achieve in a producing field, with so many variables changing continuously. In many cases, however, there should be possible a set of similar conditions, such as production performance before and after stimulation, that should be completely reported. As mentioned above, there should be full reporting of the operations of all nearby wells, so that questions of similarity can be fully addressed and answered.

What if the stimulation includes complex phenomena?

Consider the case in which the stimulating tool performs two different functions. In this case, it would be important to operate the tool with each of the functions running, separately, to study the mechanism and to validate or substantiate claims. For example, if the tool involves injection of fluid and sonic stimulation simultaneously, then it is important to study the stimulation effect of the injection alone, and of the sonic component alone (perhaps by running in unperforated casing), as well as the two components together. It is not scientifically sufficient to simply make material-balance arguments in the absence of a rigorous test.

Can different tools be tested sequentially?

It will be difficult to test different tools under identical conditions of production. It is quite possible that one tool will have affected the near-wellbore area of the stimulation well, such that the subsequent tool would behave differently from having been used in that same well had it not undergone earlier stimulation. This possibility makes it very unlikely that there will ever be truly repeatable conditions for comparison.